

# Near-Optimal Channel Estimation for Dense Array Systems

Mingyao Cui, *Graduate Student Member, IEEE*, Zijian Zhang, *Graduate Student Member, IEEE*,  
Linglong Dai, *Fellow, IEEE*, and Kaibin Huang, *Fellow, IEEE*,

**Abstract**—By deploying a large number of antennas with sub-half-wavelength spacing in a compact space, dense array systems (DASs) can fully unleash the multiplexing-and-diversity gains of limited apertures. To acquire these gains, accurate channel state information acquisition is necessary but challenging due to the large antenna numbers. To overcome this obstacle, this paper reveals that exploiting the high spatial correlation of DAS channels is crucial while designing the observation matrix for optimal/near-optimal channel estimation. Firstly, we prove that the observation matrix design is equivalent to a time-domain duality of multiple-input multiple-output precoding, which can be ideally addressed by the water-filling principle. For practical realizations, a novel ice-filling algorithm is proposed to design amplitude-and-phase controllable observation matrices, and a majorization-minimization algorithm is proposed to address the phase-only controllable case. Particularly, we prove that the ice-filling algorithm can be viewed as a “quantized” water-filling algorithm. To support the sub-optimality of the proposed designs, we provide comprehensive analyses on the achievable mean square errors and their asymptotic expressions. Finally, numerical simulations verify that our proposed channel estimation designs can achieve the near-optimal performance and outperform existing approaches significantly.

**Index Terms**—Estimation theory, mutual-information maximization, dense array systems (DAS), Bayesian regression.

## I. INTRODUCTION

From 3G to 5G, antenna array systems play an irreplaceable role in wireless communications [1]–[3]. By strategically configuring multiple antennas, an antenna array can constructively manipulate the radiated signals, allowing for enhanced wireless coverage, improved spectral efficiency, and reduced power consumption [4]–[6]. The performance of arrays continuously improves with the number of antennas [7], [8]. However, in practical scenarios, the space available for antenna deployment is usually limited, which restricts the performance gains endowed by antenna arrays [9]. To achieve a better performance with a spatially-limited aperture, dense array systems (DASs) have attracted extensive attentions in recent years [10].

Generally, DASs represent a series of array technologies that massive sub-wavelength antennas are densely arranged within a compact space. Unlike the conventional arrays with half-wavelength antenna spacing  $\lambda/2$ , the antenna spacing of DASs is much smaller, such as  $\lambda/6$  [11],  $\lambda/8$  [12],  $\lambda/10$

[13], or even  $\lambda/23$  [14]. With an increased number of sub-channels, DASs promise to achieve high array gains and fully exploit the multiplexing-and-diversity gains of limited apertures [10]. Besides, DASs can also reduce the grating lobes and provide high performance for large values of oblique angles of incidence [15]. Some works also report their advantages of super-bandwidth and super-directivity [16]–[18]. The typical DAS realizations include holographic multiple-input multiple-output (MIMO) [19], reconfigurable intelligent surfaces (RISs) [20], [21], reconfigurable holographic surfaces (RHSs) [22], fluid antenna systems [23], [24], graphene-based nano-antenna arrays [25], and so on. For example, in [11], massive sub-wavelength patches of  $\lambda/6$ -spacing are densely printed on a holographic MIMO surface to generate multiple beams flexibly. In [26], meta-elements sized of  $\lambda/2.5 \times \lambda/17.5$  are seamlessly integrated onto a feeding microstrip to achieve RHS beam steering. In [14], an RIS composed of antennas sized of  $\lambda/23 \times \lambda/23$  is designed and fabricated for terahertz communications.

The performance gains of antenna arrays are realized via the constructive beamformers enabled by their phase shifters and radio frequency (RF) chains. To realize effective beamforming and signal demodulation, the acquisition of accurate channel state information (CSI) is essential. Up to now, many estimators have been proposed to acquire the CSI of large antenna arrays. Their fundamental principle involves receiving pilot signals using observation matrices and recovering the channel by advanced estimation algorithms. For example, when the available pilot length is larger than the antenna number, the classical non-parametric algorithms are widely used, including least square (LS) estimator and minimum mean square error (MMSE) estimator. Leveraging the property of channel sparsity, compressed sensing (CS)-based channel estimators are widely studied to improve the estimation accuracy and reduce the pilot overhead [27], [28], such as the orthogonal matching pursuit (OMP)-based estimator [29], the message passing (MP)-based estimator [30]–[32], and the gridless sparse signal reconstructor [33]. By training neural networks with a large amounts of channel data, the deep learning approaches are also utilized to realize data-driven channel estimators [34], [35]. Besides, beam alignment techniques [36]–[38], including beam sweeping and hierarchical beam training, have also been widely explored to acquire the implicit CSI with low pilot overhead.

Although most of existing channel estimators can be adopted in DASs, they fail to fully exploit the high spatial correlation of DAS channels, thereby leaving a remarkable performance gap from the optimal estimator. Specifically, this

Mingyao Cui and Kaibin Huang are with the Department of Electrical and Electronic Engineering, The University of Hong Kong, Hong Kong (e-mails: mycui@eee.hku.hk, huangkb@eee.hku.hk).

Zijian Zhang and Linglong Dai are with the Department of Electronic Engineering, Tsinghua University, Beijing 100084, China, as well as the Beijing National Research Center for Information Science and Technology (BNRist), Beijing 100084, China (e-mails: zhangzj20@mails.tsinghua.edu.cn, daill@tsinghua.edu.cn).

spatial correlation is attributed to the fact that, the extremely-dense deployment of DAS antennas significantly increases the similarity of radio waves impinging on antenna ports and aggravates the mutual-coupling effect between adjacent antenna circuits. From the mathematical perspective, this fact implies that the covariance matrices of DAS channels are no longer diagonal, but highly structured and/or under-determined. For diagonal covariance matrices, a uniform or random pilot-sensing strategy is sufficient to achieve the optimality of estimation [39], [40]. Thereby, in conventional channel estimations, the observation matrices for receiving the pilot signals are either generated randomly or set as predefined codebooks, such as the Discrete Fourier Transform (DFT) matrix and the identity matrix [27]–[31], [33]–[37]. In contrast, since the correlation matrix of DAS channels are full of structural features, it is believed that their observation matrices can be tightly aligned with these features in pilot transmission. This structured pilot-sensing process has a high potential to remarkably boost the channel estimation accuracy in DASs [41]–[43].

To achieve this goal, our work represents the first attempt on designing and analyzing the optimal/near-optimal observation matrices in the DAS channel estimation. By incorporating a mutual-information-maximization (MIM)-enabled observation matrix design into a Bayesian regression-based estimator, we propose a novel framework for DAS channel estimation. Our main contributions are summarized as follows.

- **Framework of DAS channel estimator:** From the perspective of MIM, the proposed framework of DAS channel estimation establishes the connection between channel estimation and MIMO precoding. Specifically, we propose to design the DAS’s observation matrix by minimizing the information uncertainty between the received pilots and wireless channels. The formulated MIM problem for observation matrix design is shown to be a time-domain duality of MIMO precoding design. In particular, the multi-RF-chain resources for precoding design is transformed to the multi-timeslot-pilot resources for channel estimation. Motivated by this finding, we prove that the ideal (but maybe unachievable in practice) observation matrix follows the water-filling principle, which is built by the eigenvectors of the channel’s covariance matrix followed by the optimal power allocation.
- **Ice-filling enabled observation matrix design:** For practical DAS channel estimations, the continuous power-allocation by water-filling is not applicable as the pilot length is discrete and each pilot transmission has independent power constraint. To deal with this issue, we propose an ice-filling algorithm to design the amplitude-and-phase controllable observation matrices. This algorithm sequentially generates the optimal blocks of the observation matrix by maximizing the mutual information (MI) increment between two adjacent pilot transmissions. An important insight is that the ice-filling algorithm converts the *power-allocation-process* of the ideal water-filling algorithm into an *eigenvector-assignment-process*. We rigorously prove that, the continuous powers allocated

by water-filling are quantized as the number of times that *each eigenvector of the channel covariance is assigned for pilot transmission* by ice-filling, with a quantization error smaller than one. The proven quantization nature thereby ensures the near-optimality of the proposed ice-filling algorithm.

- **Majorization minimization (MM) enabled observation matrix design:** We then apply our framework for DAS channel estimation to analog combining/beamforming architecture. In this context, only the phases of the observation matrix’s weights are controllable while their amplitudes are fixed, making both the ice-filling and water-filling algorithms invalid. To address this challenge, we propose a MM algorithm for designing the observation matrix. Its novelty lies in replacing the primal non-convex MIM problem with a series of tractable approximate subproblems having analytical solutions, which are solved in an alternating optimization manner. Numerical simulations demonstrate that its channel estimation performance is comparable to the sub-optimal ice-filling algorithm.
- **Performance analysis:** Comprehensive analyses on the achievable mean square errors (MSEs) are provided to validate the effectiveness of the proposed designs. We analytically prove that, compared to the random observation matrix design, the ice-filling algorithm can significantly improve the estimation accuracy by the order of the ratio between the number of antennas and the rank of channel covariance. Furthermore, based on the derived quantization nature of ice-filling, the MSE gap between water-filling and ice-filling is proved to decay quadratically with the pilot length, demonstrating the near-optimality of the ice-filling algorithm. In addition, the close-form MSEs under imperfect channel covariance are also derived. The superiority of the proposed algorithms is further validated using numerical results under both perfect and imperfect channel covariance conditions.

The remainder of the paper is organized as follows. The system model and problem formulation are presented in Section II. The proposed framework of channel estimation design is given in Section III. The practical observation matrix designs are elaborated in Section IV. Then, the MSEs are analyzed in Section V. Simulation results are carried out in Section VI, and finally the conclusions are drawn in Section VII.

*Notation:* Lower-case and upper-case boldface letters represent vectors and matrices, respectively.  $[\cdot]^{-1}$ ,  $[\cdot]^\dagger$ ,  $[\cdot]^*$ ,  $[\cdot]^T$ , and  $[\cdot]^H$  denote the inverse, pseudo-inverse, conjugate, transpose, and conjugate-transpose operations, respectively;  $\|\cdot\|_2$  denotes the  $l_2$ -norm of the argument;  $\|\cdot\|_F$  denotes the Frobenius norm of the argument;  $|\cdot|$  denotes the element-wise amplitude of its argument;  $\text{Tr}(\cdot)$  denotes the trace operator;  $\mathbb{E}(\cdot)$  is the expectation operator;  $\Re\{\cdot\}$  denotes the real part of the argument;  $\lambda_{\max}(\cdot)$  denotes the largest eigenvalue of its argument;  $\mathcal{CN}(\boldsymbol{\mu}, \boldsymbol{\Sigma})$  denotes the complex Gaussian distribution with mean  $\boldsymbol{\mu}$  and covariance  $\boldsymbol{\Sigma}$ ;  $\mathcal{U}(a, b)$  denotes the uniform distribution between  $a$  and  $b$ ;  $\mathbf{I}_L$  is an  $L \times L$  identity matrix;  $\mathbf{1}_L$  is an  $L$ -dimensional all-one vector; and  $\mathbf{0}_L$  is an all-zero

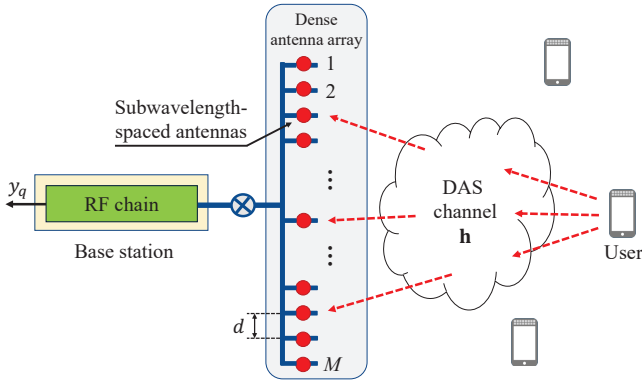


Fig. 1. An illustration of channel estimation for an DAS, where one  $M$ -antenna BS receives the pilots from a user in the uplink.

vector or matrix with dimension  $L$ .

## II. SYSTEM MODEL

This paper commences by elaborating on the system model. As illustrated in Fig. 1, we focus on the narrowband channel estimation of an uplink single-input multiple-output (SIMO) system, which comprises an  $M$ -antenna BS equipped with one RF chain and a single-antenna user [7].

Let  $\mathbf{h} \in \mathbb{C}^{M \times 1}$  denote the narrowband channel vector associated with  $M$  densely deployed antennas, and  $Q$  denote the number of transmit pilots within a coherence-time frame. The received signal  $y_q \in \mathbb{C}$  at the BS in timeslot  $q$  is modeled as

$$y_q = \mathbf{w}_q^H \mathbf{h} s_q + \mathbf{w}_q^H \mathbf{z}_q, \quad (1)$$

where  $\mathbf{w}_q \in \mathbb{C}^{M \times 1}$  is the observation vector at the BS,  $s_q$  the pilot transmitted by the user, and  $\mathbf{z}_q \sim \mathcal{CN}(\mathbf{0}_M, \sigma^2 \mathbf{I}_M)$  the additive white Gaussian noise. As the observation vector  $\mathbf{w}_q$  affects both the desired signal  $\mathbf{h} s_q$  and the noise  $\mathbf{z}_q$ , its power has no impact on the estimation accuracy. Therefore, without any loss of generality, we can normalize  $\mathbf{w}_q$  to  $\|\mathbf{w}_q\|_2 = 1$ , which reshapes the noise distribution to  $\mathbf{w}_q^H \mathbf{z}_q \sim \mathcal{CN}(0, \sigma^2)$ . For ease of notation, we assume that  $s_q = 1$  for all  $q \in \{1, \dots, Q\}$ .

As shown in Fig. 2, in each timeslot, the BS reconfigures its observation vector to obtain sufficient observations. Considering the total  $Q$  timeslots for pilot transmission, we get

$$\mathbf{y} = \mathbf{W}^H \mathbf{h} + \mathbf{z}, \quad (2)$$

where  $\mathbf{y} = [y_1, \dots, y_Q]^T$ ,  $\mathbf{W} = [\mathbf{w}_1, \dots, \mathbf{w}_Q]$  stands for the observation matrix, and  $\mathbf{z} := [\mathbf{w}_1^H \mathbf{z}_1, \dots, \mathbf{w}_Q^H \mathbf{z}_Q]^T \sim \mathcal{CN}(0, \sigma^2 \mathbf{I}_Q)$ . The goal of channel estimation is to recover the channel  $\mathbf{h}$  from the received pilot  $\mathbf{y}$ . In particular, the Bayesian estimation criterion promises to minimize the MSE,  $E\|\mathbf{h} - \hat{\mathbf{h}}\|_2^2$ , by designing the reconstructor  $\hat{\mathbf{h}}$  as a function of  $\mathbf{y}$  and our prior knowledge to  $\mathbf{h}$ .

In existing literature, a significant amount of effort has endeavored to design advanced reconstructors for making the estimation of  $\mathbf{h}$  as accurate as possible, such as CS algorithms and deep-learning based methods [27]–[31], [33]–[35]. However, the design of the observation matrix,  $\mathbf{W}$ , for channel estimation is largely unexplored. It is worth noting that the

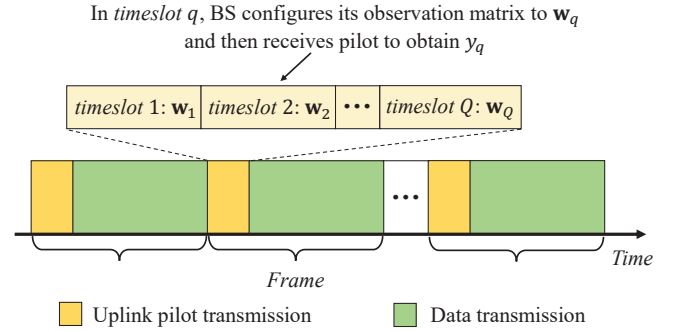


Fig. 2. The frame structure for DAS channel estimation.

extremely high spatial correlation exhibited by DAS channels leads to a remarkable deviation of the channel covariance matrix from the identity matrix. This deviation highlights the significance of aligning the observation matrix with the channel's subspace for boosting the estimation accuracy. Motivated by this fact, this paper proposes to optimize the reconstructor and the observation matrix jointly, i.e.,

$$\min_{\hat{\mathbf{h}}, \mathbf{W} \in \mathcal{W}} E\|\mathbf{h} - \hat{\mathbf{h}}\|_2^2, \quad (3)$$

where  $\mathcal{W}$  stands for the feasible set of the observation matrix  $\mathbf{W}$ . For instance, let's consider the  $q$ -th observation vector,  $\mathbf{w}_q$ , from the matrix  $\mathbf{W}$ . In the case of amplitude-and-phase controllable scenarios, the constraint imposed on  $\mathbf{w}_q$  is  $\|\mathbf{w}_q\|_2 = 1$ ; while in the case of phase-only controllable scenarios [44], each entry of  $\mathbf{w}_q$  is subject to the constant modulus constraint, i.e.,  $|w_{q,m}| = \frac{1}{\sqrt{M}}$  for  $m \in \{1, 2, \dots, M\}$ .

## III. MUTUAL INFORMATION MAXIMIZATION FOR CHANNEL ESTIMATION IN DASS

This section presents a MIM based method to solve the problem outlined in (3). We first establish a general framework of the proposed design. A water-filling-inspired observation-matrix-design is then investigated as an ideal case of the proposed framework.

### A. Framework of the Proposed Channel Estimation Design

The framework of our proposed channel estimator is illustrated in Fig. 3. It consists of two stages: the MIM enabled observation matrix design and the Bayesian regression based channel estimation, each of which is explained in detail below.

1) *Bayesian regression based channel estimation*: As previously discussed, a dense array features highly correlated channels across different antenna ports, which motivates us to recover  $\mathbf{h}$  using Bayesian regression. Suppose the channel,  $\mathbf{h}$ , is sampled from a Gaussian process  $\mathcal{CN}(\mathbf{0}_M, \Sigma_{\mathbf{h}})$ . The covariance matrix  $\Sigma_{\mathbf{h}} \in \mathbb{C}^{M \times M}$  characterizes our prior knowledge to the *kernel* of channel, which is thus referred to as the *prior kernel* in the sequel. Given the Gaussian distributions of the channel and noise, the joint probability distribution of  $[\mathbf{h}^T, \mathbf{y}^T]^T$  is

$$\mathcal{CN}\left(\begin{bmatrix} \mathbf{0}_M \\ \mathbf{0}_Q \end{bmatrix}, \begin{bmatrix} \Sigma_{\mathbf{h}} & \Sigma_{\mathbf{h}} \mathbf{W} \\ \mathbf{W}^H \Sigma_{\mathbf{h}} & \mathbf{W}^H \Sigma_{\mathbf{h}} \mathbf{W} + \sigma^2 \mathbf{I}_Q \end{bmatrix}\right). \quad (4)$$

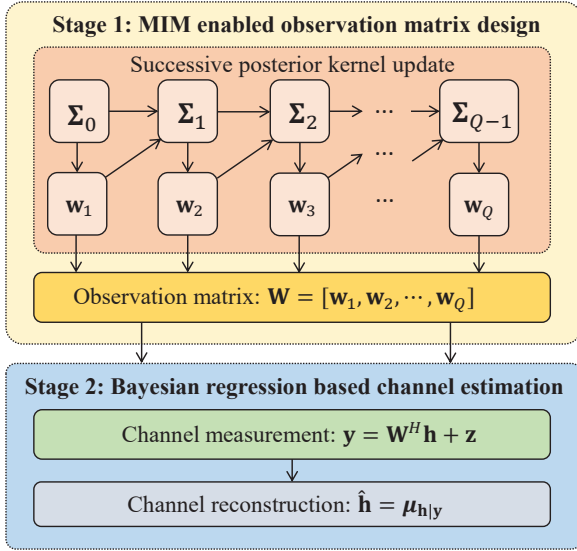


Fig. 3. Framework of the proposed channel estimation method.

Thereby, the posterior mean and posterior covariance of  $\mathbf{h}$  can be calculated as:

$$\mu_{\mathbf{h}|\mathbf{y}} = \Sigma_{\mathbf{h}} \mathbf{W} (\mathbf{W}^H \Sigma_{\mathbf{h}} \mathbf{W} + \sigma^2 \mathbf{I}_Q)^{-1} \mathbf{y}, \quad (5)$$

$$\Sigma_{\mathbf{h}|\mathbf{y}} = \Sigma_{\mathbf{h}} - \Sigma_{\mathbf{h}} \mathbf{W} (\mathbf{W}^H \Sigma_{\mathbf{h}} \mathbf{W} + \sigma^2 \mathbf{I}_Q)^{-1} \mathbf{W}^H \Sigma_{\mathbf{h}}. \quad (6)$$

For an arbitrary observation matrix  $\mathbf{W}$ , the optimal Bayesian estimation of  $\mathbf{h}$  is thus the posterior mean  $\mu_{\mathbf{h}|\mathbf{y}}$ , i.e.,  $\hat{\mathbf{h}} = \mu_{\mathbf{h}|\mathbf{y}}$ . In the subsequent discussion,  $\Sigma_{\mathbf{h}|\mathbf{y}}$  is also referred to as the *posterior kernel*.

2) *MIM enabled observation matrix design*: It is evident that the posterior kernel  $\Sigma_{\mathbf{h}|\mathbf{y}}$  relies heavily on the choice of the observation matrix  $\mathbf{W}$ . This fact implies that customizing an observation matrix  $\mathbf{W}$  to the kernel structure of a dense array channel can significantly reduce the estimation error, as measured by  $E\|\mathbf{h} - \hat{\mathbf{h}}\|_2^2 = \text{Tr}(\Sigma_{\mathbf{h}|\mathbf{y}})$ . Unfortunately, the direct optimization of  $\text{Tr}(\Sigma_{\mathbf{h}|\mathbf{y}})$  is non-convex and intractable, making it hard to gain insights from this optimization process. To overcome this challenge, we adopt the idea of Gaussian Process Regression to design  $\mathbf{W}$  from the perspective of MIM [41]–[43]. Specifically, the main objective of Gaussian Process Regression is to extract as much information about the unknown channel  $\mathbf{h}$  from the observation  $\mathbf{y}$  as possible. Accordingly, the observation matrix,  $\mathbf{W}$ , is designed to maximize the MI between  $\mathbf{y}$  and  $\mathbf{h}$ :

$$\begin{aligned} \max_{\mathbf{W} \in \mathcal{W}} I(\mathbf{y}; \mathbf{h}) &= H(\mathbf{y}) - H(\mathbf{y}|\mathbf{h}) \\ &= \log \det \left( \mathbf{I}_M + \frac{1}{\sigma^2} \mathbf{W}^H \Sigma_{\mathbf{h}} \mathbf{W} \right), \end{aligned} \quad (7)$$

where  $I(\cdot; \cdot)$  denotes the MI;  $H(\cdot)$  denotes the entropy of its argument; and  $\det(\cdot)$  denotes the determinant of its argument. It is notable that the observation matrix design in (7) resembles the well-know single-user MIMO precoding problem [45]. Comprehensive comparisons between these two methodologies are provided below.

- **Category of unknown data**: Both MIMO precoding and observation matrix design in (7) aim to reduce the uncer-

tainty between the received data,  $\mathbf{y}$ , and the unknown data. The former methodology regards the transmitted symbol vector, denoted by  $\mathbf{x}$ , as the unknown data. To facilitate MIMO precoding, *multiple RF chains* are employed to support an equal number of data streams [45]. On the other hand, the unknown data to the latter methodology is the channel,  $\mathbf{h}$ . During channel estimation, especially in our considered system, *a single RF chain accompanied by repeated pilot transmission in multiple timeslots* is required to recover  $\mathbf{h}$ . In comparison, one can discover that the multiple RF chains in MIMO precoding are converted to the multi-timeslot pilot resources in channel estimation. Thereby, the design of the observation matrix in (7) can be viewed as a time-domain duality of classic MIMO precoding.

- **Constraint on the observation matrix**: The mathematical difference between MIMO precoding and observation matrix design is primarily attributed to the constraints imposed on  $\mathbf{W}$ . For MIMO precoding, each column of  $\mathbf{W}$  refers to a precoding vector associated with one dedicated RF chain. The optimization of precoding vectors, leveraging multiple RF chains, typically enforces the *total-power-constraint* on  $\mathbf{W}$ , i.e.,  $\|\mathbf{W}\|_F^2 = Q$ . In terms of the observation matrix design, each column of  $\mathbf{W}$  signifies an observation vector used for receiving one pilot signal. As discussed in Section II, since each observation vector  $\mathbf{w}_q$  amplifies both the desired signal and the noise, it is subject to the pilot-wise power constraint, i.e.,  $\|\mathbf{w}_q\|_2^2 = 1$  or  $|w_{q,m}| = \frac{1}{\sqrt{M}}$  [27]. As a result, the distinction in the observation matrix constraint differentiates the MIM in (7) from the classic MIMO precoding.

To summarize, the proposed channel estimation strategy, as illustrates in Fig. 3, involves obtaining the optimal observation matrix by solving the MIM problem (7), performing pilot transmissions as presented in (2), and finally recovering the channel  $\mathbf{h}$  using the Bayesian regression (5). It is evident that the main technical challenge in our framework comes from solving the MIM problem defined in (7).

### B. Water-Filling Inspired Ideal Observation Matrix Design

To help understanding of the proposed framework, we relax the pilot-wise power constraint,  $\|\mathbf{w}_q\|_2^2 = 1$ , to the total power constraint,  $\|\mathbf{W}\|_F^2 = \sum_{q=1}^Q \|\mathbf{w}_q\|_2^2 = Q$ , to derive an ideal solution to the MIM problem in (7). Note that the feasible set built on  $\|\mathbf{w}_q\|_2^2 = 1$  is a subset of that established by  $\sum_{q=1}^Q \|\mathbf{w}_q\|_2^2 = Q$ . Thereby, the derived ideal solution is practically unachievable but can serve as an upper-bound for estimation accuracy evaluation. In this context, the problem (7) is transformed to the well-known single-user MIMO precoding problem, which can be globally optimized using the water-filling principle [46] as summarized in **Algorithm 1**.

Specifically, let the eigenvalue decomposition of  $\Sigma_{\mathbf{h}}$  be  $\mathbf{U}_K \Lambda_K \mathbf{U}_K^H$ , where  $K$  is the rank of  $\Sigma_{\mathbf{h}}$ ,  $\mathbf{U}_K = [\mathbf{u}_1, \mathbf{u}_2, \dots, \mathbf{u}_K]$  encompasses the eigenvectors, and  $\Lambda_K = \text{diag}\{\lambda_1, \lambda_2, \dots, \lambda_K\}$  represents the positive eigenvalues in a descending order. The water-filling algorithm dictates that the optimal observation matrix  $\mathbf{W}$  is constructed by the

**Algorithm 1** Water-Filling-Based Observation Matrix Design**Input:** Number of pilots  $Q$ , prior kernel  $\Sigma_{\mathbf{h}}$ .**Output:** Designed observation matrix  $\mathbf{W}$ .

- 1: Eigenvalue decomposition:  $\Sigma_{\mathbf{h}} = \mathbf{U}_K \Lambda_K \mathbf{U}_K^H$
- 2: Perform water-filling to get  $\mathbf{P}$  by (8)
- 3: Construct observation matrix:  $\mathbf{W} = \mathbf{U}_K \mathbf{P}$
- 4: **return** Designed observation matrix  $\mathbf{W}$

eigenvectors allocated by different powers, i.e.,  $\mathbf{W} = \mathbf{U}_K \mathbf{P}$ , with  $\mathbf{P} \in \mathbb{R}^{K \times Q}$  representing the power allocation matrix. We assume that the pilot length  $Q$  is larger than the rank  $K$ . Then power allocation matrix is expressed as  $\mathbf{P} = [\mathbf{P}_K, \mathbf{0}_{K \times (Q-K)}]$  with  $\mathbf{P}_K = \text{diag}\{\sqrt{p_1}, \sqrt{p_2}, \dots, \sqrt{p_K}\}$ . The power  $p_k$  allocated to each eigenvector is calculated by the water-filling principle:

$$p_k = \left( \beta - \frac{\sigma^2}{\lambda_k} \right)^+, \forall k \in \{1, 2, \dots, K\}, \quad (8)$$

where the water-level  $\beta$  can be efficiently determined via binary search to meet the total power constraint:  $\sum_{k=1}^K \left( \beta - \frac{\sigma^2}{\lambda_k} \right)^+ = Q$ .

## IV. PRACTICAL OBSERVATION MATRIX DESIGN

This section elaborates on the observation matrix design in practical scenarios. Firstly, a greedy-method based principle is leveraged to solve the MIM problem in (7). Building on this principle, we propose an ice-filling algorithm for designing the amplitude-and-phase controllable observation matrices. Additionally, we conduct a comprehensive analysis on the relationship between ice-filling and water-filling. Subsequently, a MM-based algorithm is proposed for the design of phase-only controllable observation matrices.

## A. Observation Matrix Design Using Greedy Method

In practical pilot transmission scenarios where the pilot-wise power constraint is imposed, the MIM problem in (7) is non-convex since the objective function is non-concave with respect to (w.r.t)  $\mathbf{W}$ . To overcome this obstacle, we harness a greedy method to obtain the observation vectors in a pilot-by-pilot manner. Specifically, we define  $\mathbf{W}_t = [\mathbf{w}_1, \mathbf{w}_2, \dots, \mathbf{w}_t]$  as the observation matrix for timeslots  $1 \sim t$ , where  $t < Q$ , and denote  $\mathbf{y}_t = \mathbf{W}_t^H \mathbf{h} + \mathbf{z}_t$  as the corresponding received signal. Given the current observation matrix  $\mathbf{W}_t$ , our greedy method aims to determine the next observation vector,  $\mathbf{w}_{t+1}$ , by maximizing the MI increment from timeslot  $t$  to  $t+1$ , i.e.,  $\max_{\mathbf{w}_{t+1}} I(\mathbf{y}_{t+1}; \mathbf{h}) - I(\mathbf{y}_t; \mathbf{h})$ . As proved in Appendix A, the MI increment is expressed as

$$I(\mathbf{y}_{t+1}; \mathbf{h}) - I(\mathbf{y}_t; \mathbf{h}) = \log_2 \left( 1 + \frac{1}{\sigma^2} \mathbf{w}_{t+1}^H \Sigma_t \mathbf{w}_{t+1} \right), \quad (9)$$

where  $\Sigma_t$  represents the posterior kernel matrix of  $\mathbf{h}$  given the observation  $\mathbf{y}_t$ , i.e.,

$$\Sigma_t = \Sigma_{\mathbf{h}} - \Sigma_{\mathbf{h}} \mathbf{W}_t (\mathbf{W}_t^H \Sigma_{\mathbf{h}} \mathbf{W}_t + \sigma^2 \mathbf{I}_t)^{-1} \mathbf{W}_t^H \Sigma_{\mathbf{h}}. \quad (10)$$

**Algorithm 2** Ice-Filling-Based Observation Matrix Design**Input:** Number of pilots  $Q$ , kernel  $\Sigma_{\mathbf{h}}$ .**Output:** Designed observation matrix  $\mathbf{W}$ .

- 1: Find the eigenvectors  $[\mathbf{u}_1, \mathbf{u}_2, \dots, \mathbf{u}_K]$  and the corresponding eigenvalues  $[\lambda_1, \lambda_2, \dots, \lambda_K]$  of  $\Sigma_0 = \Sigma_{\mathbf{h}}$
- 2: Initialize:  $[\lambda_1^0, \lambda_2^0, \dots, \lambda_K^0] = [\lambda_1, \lambda_2, \dots, \lambda_K]$
- 3: **for**  $t = 0, \dots, Q - 1$  **do**
- 4:  $k_t = \arg \max_{k \in \{1, 2, \dots, K\}} \{\lambda_k^t\}$
- 5: Eigenvector-assignment:  $\mathbf{w}_{t+1} = \mathbf{u}_{k_t}$
- 6: Eigenvalue-update:  $\lambda_{k_t}^{t+1} = \frac{\lambda_{k_t}^t \sigma^2}{\lambda_{k_t}^t + \sigma^2}$
- 7: Eigenvalue-preserve:  $\lambda_k^{t+1} = \lambda_k^t$  with  $k \in \{1, 2, \dots, K\} - k_t$
- 8: **end for**
- 9: Construct observation matrix:  $\mathbf{W} = [\mathbf{w}_1, \mathbf{w}_2, \dots, \mathbf{w}_Q]$
- 10: **return** Designed observation matrix  $\mathbf{W}$

Thereafter, the optimal  $\mathbf{w}_{t+1}$  can be attained by solving the following quadratic problem:

$$\mathbf{w}_{t+1} = \underset{\mathbf{w} \in \mathcal{W}}{\text{argmax}} \mathbf{w}^H \Sigma_t \mathbf{w}. \quad (11)$$

Before delving into the detail this problem, it is notable that repeatedly calculating the inverse of  $\mathbf{W}_t^H \Sigma_{\mathbf{h}} \mathbf{W}_t + \sigma^2 \mathbf{I}_t$  in each timeslot  $t$  is necessary for obtaining the kernel  $\Sigma_t$  in (10) and (11). To avoid these computationally inefficient matrix-inversion operations, **Lemma 1** is derived to offer an efficient approach to calculate  $\Sigma_t$ .

**Lemma 1:**  $\Sigma_t$  can be calculated from  $\Sigma_{t-1}$  and  $\mathbf{w}_t$  as:

$$\Sigma_t = \Sigma_{t-1} - \frac{\Sigma_{t-1} \mathbf{w}_t \mathbf{w}_t^H \Sigma_{t-1}}{\mathbf{w}_t^H \Sigma_{t-1} \mathbf{w}_t + \sigma^2}. \quad (12)$$

*Proof:* See Appendix B. ■

Clearly, **Lemma 1** reveals the relationship between  $\Sigma_t$  and  $\Sigma_{t-1}$ , and thereby allowing us to update  $\Sigma_t$  from  $\Sigma_{t-1}$  without the need for matrix inversion.

As a result, equations (9) to (12) inspire us to propose the framework presented in Fig. 3 for the design of observation matrix. The framework begins with setting  $\Sigma_0$  as the prior kernel of the channel,  $\Sigma_{\mathbf{h}}$ . The first observation vector  $\mathbf{w}_1$  is then obtained by solving the quadratic problem in (11). For subsequent timeslots  $t$  ( $t \in \{1, 2, \dots, Q - 1\}$ ), the posterior kernels  $\Sigma_t$  are updated from  $\Sigma_{t-1}$  and  $\mathbf{w}_t$  using **Lemma 1**. The update of the posterior kernels then triggers the update of the observation vectors  $\mathbf{w}_{t+1}$  by solving problem (11) pilot-by-pilot. These two updating steps are repeated until all  $Q$  observation vectors are generated for performing the ensuing Bayesian regression.

In the sequel, we will elaborate on solving problem (11) under the amplitude-and-phase controllable and phase-only controllable cases, respectively, to complete the design of observation matrix.

## B. Ice-Filling for Amplitude-and-Phase Controllable Observation Matrix

For amplitude-and-phase controllable observation matrices, problem (11) can be formulated as the well-known Rayleigh

quotient problem:

$$\mathbf{w}_{t+1} = \underset{\|\mathbf{w}\|_2=1}{\operatorname{argmax}} \mathbf{w}^H \boldsymbol{\Sigma}_t \mathbf{w}. \quad (13)$$

where the principal eigenvector of  $\boldsymbol{\Sigma}_t$  yields the optimal solution to  $\mathbf{w}_{t+1}$ , i.e.,  $\boldsymbol{\Sigma}_t \mathbf{w}_{t+1} = \lambda_{\max}(\boldsymbol{\Sigma}_t) \mathbf{w}_{t+1}$ . By combining the updating strategy of  $\boldsymbol{\Sigma}_t$  described in **Lemma 1** and the property of the principal eigenvector  $\mathbf{w}_{t+1}$ , we can prove **Theorem 1**, which lays the foundation for our ice-filling algorithm in designing amplitude-and-phase controllable observation matrices.

**Theorem 1:** If  $\mathbf{w}_t$  is the principal eigenvector of  $\boldsymbol{\Sigma}_{t-1}$ , then  $\boldsymbol{\Sigma}_t$  can be rewritten as

$$\boldsymbol{\Sigma}_t = \boldsymbol{\Sigma}_{t-1} - \frac{\lambda_{\max}^2(\boldsymbol{\Sigma}_{t-1})}{\lambda_{\max}(\boldsymbol{\Sigma}_{t-1}) + \sigma^2} \mathbf{w}_t \mathbf{w}_t^H. \quad (14)$$

*Proof:* Applying the property of the principal eigenvector  $\boldsymbol{\Sigma}_{t-1} \mathbf{w}_t = \lambda_{\max}(\boldsymbol{\Sigma}_{t-1}) \mathbf{w}_t$ , we get  $\mathbf{w}_t^H \boldsymbol{\Sigma}_{t-1} \mathbf{w}_t = \lambda_{\max}(\boldsymbol{\Sigma}_{t-1})$  and  $\boldsymbol{\Sigma}_{t-1} \mathbf{w}_t \mathbf{w}_t^H \boldsymbol{\Sigma}_{t-1} = \lambda_{\max}^2(\boldsymbol{\Sigma}_{t-1}) \mathbf{w}_t \mathbf{w}_t^H$ , which together with **Lemma 1** give rise to (14). ■

**Remark 1:** Given that  $\mathbf{w}_t$  is the principal eigenvector of  $\boldsymbol{\Sigma}_{t-1}$ , **Theorem 1** implies that the posterior kernels,  $\boldsymbol{\Sigma}_t$  and  $\boldsymbol{\Sigma}_{t-1}$ , share the identical eigenspace. This fact immediately leads to the result that, for the amplitude-and-phase controllable observation matrix, the eigenvectors,  $\{\mathbf{u}_k\}$ , of the prior kernel,  $\boldsymbol{\Sigma}_0 = \boldsymbol{\Sigma}_h$ , are inherited by all subsequent posterior kernels,  $\boldsymbol{\Sigma}_1, \boldsymbol{\Sigma}_2, \dots$ , and  $\boldsymbol{\Sigma}_{Q-1}$ . Thereby, we can draw the conclusion that all observation vectors,  $\{\mathbf{w}_t\}$ , are picked from the eigenvectors of  $\boldsymbol{\Sigma}_h$ .

**Remark 2:** In terms of the eigenvalues when updating  $\boldsymbol{\Sigma}_{t-1}$  to  $\boldsymbol{\Sigma}_t$ , it can be straightforwardly proved from **Theorem 1** that only the principal eigenvalue,  $\lambda_{\max}(\boldsymbol{\Sigma}_{t-1})$ , of  $\boldsymbol{\Sigma}_{t-1}$  is squeezed to an eigenvalue of  $\boldsymbol{\Sigma}_t$  given by

$$\lambda_{\max}(\boldsymbol{\Sigma}_{t-1}) - \frac{\lambda_{\max}^2(\boldsymbol{\Sigma}_{t-1})}{\lambda_{\max}(\boldsymbol{\Sigma}_{t-1}) + \sigma^2} = \frac{\lambda_{\max}(\boldsymbol{\Sigma}_{t-1})\sigma^2}{\lambda_{\max}(\boldsymbol{\Sigma}_{t-1}) + \sigma^2}, \quad (15)$$

while the other eigenvalues are preserved.

As a result, updating kernels in amplitude-and-phase controllable situations is equivalent to squeezing the eigenvalues within the identical eigenspace.

Motivated by **Theorem 1**, our proposed ice-filling algorithm is intrinsically an *eigenvector-assignment-process*, as presented in **Algorithm 2**. To elaborate, we define  $\{\lambda_1^t, \lambda_2^t, \dots, \lambda_K^t\}$  as the eigenvalues of the posterior kernel  $\boldsymbol{\Sigma}_t$ , which are initialized as the eigenvalues of the prior kernel  $\boldsymbol{\Sigma}_h$  in Step 2. In each timeslot, we identify the largest eigenvalue from  $\{\lambda_1^t, \lambda_2^t, \dots, \lambda_K^t\}$  and index it by  $k_t$  in Step 4. Then, the corresponding eigenvector  $\mathbf{u}_{k_t}$  of  $\boldsymbol{\Sigma}_h$ , which is equivalent to the principal eigenvector of  $\boldsymbol{\Sigma}_t$ , is assigned to  $\mathbf{w}_{t+1}$  in Step 5. Finally, according to **Theorem 1**, the selected eigenvalue  $\lambda_{k_t}^t$  is squeezed to  $\frac{\lambda_{k_t}^t \sigma^2}{\lambda_{k_t}^t + \sigma^2}$ , while the other eigenvalues of  $\boldsymbol{\Sigma}_t$  are preserved, to attain the eigenvalues of the next kernel  $\boldsymbol{\Sigma}_{t+1}$ . These steps are repeatedly executed until all observation vectors are generated, which completes the proposed ice-filling algorithm.

### C. Ice-Filling Versus Water-Filling

In this subsection, we put forward a more insightful interpretation to the ice-filling algorithm that establishes its connection with the water-filling principle. Generally speaking, the proposed ice-filling algorithm can be viewed as a quantization of the water-filling principle. Specifically, it is clear that the observation matrices generated by both the water-filling and the proposed ice-filling algorithms fall within the eigenspace of  $\boldsymbol{\Sigma}_h$ . The major distinction is attributed to their ‘‘power allocation strategies’’. The water-filling principle allocates  $Q$  units of power to the  $K$  eigenvectors using (8). On the other hand, the ice-filling algorithm transforms this power-allocation process into an *eigenvector-assignment process*, where the  $K$  eigenvectors are repeatedly assigned to the observation vectors in  $Q$  timeslots.

To be more precise, recall that  $p_k$  in (8) denotes the optimal power allocated to the  $k$ -th eigenvector using the water-filling principle, satisfying  $\sum_{k=1}^K p_k = Q$ . For the sake of discussion, we introduce the definition of ‘‘pilot reuse frequency’’ as follows.

**Definition 1:** The pilot reuse frequency  $n_k^t \in \mathbb{Z}^+$ , with  $k \in \{1, 2, \dots, K\}$  and  $t \in \{1, 2, \dots, Q\}$ , is defined as the number of times that the  $k$ -th eigenvector,  $\mathbf{u}_k$ , of the prior kernel is selected as the observation vector by the ice-filling algorithm during timeslots  $1 \sim t$ . The pilot reuse frequencies satisfy  $\sum_{k=1}^K n_k^t = t$ . For ease of expression, we define  $n_k := n_k^Q$  as the pilot reuse frequency during the total  $Q$  timeslots.

Comparing the definitions of  $p_k$  and  $n_k$ , we can intuitively interpret the  $n_k$ -timeslot reuse of the observation vector  $\mathbf{u}_k$  for pilot transmission as allocating  $n_k$  units of power to  $\mathbf{u}_k$ . More importantly, **Definition 1** enables us to derive the analytical expressions for the eigenvalues  $\{\lambda_k^t\}$  in **Algorithm 2**. Note that the eigenvalue update rule of the ice-filling algorithm can be rewritten as a recursive formula:

$$\lambda_{k_t}^{t+1} = \frac{\lambda_{k_t}^t \sigma^2}{\lambda_{k_t}^t + \sigma^2} \Leftrightarrow \frac{\sigma^2}{\lambda_{k_t}^{t+1}} = 1 + \frac{\sigma^2}{\lambda_{k_t}^t}, \quad (16)$$

where  $\lambda_{k_t}^t$  is the largest eigenvalue from  $\{\lambda_1^t, \lambda_2^t, \dots, \lambda_K^t\}$ . This recursive formula implies that whenever the  $k$ -th eigenvector is selected as an observation vector, the value of  $\frac{\sigma^2}{\lambda_k^t}$  increases by 1, which naturally gives rise to the close-form expression of  $\lambda_k^t$  in **Lemma 2**.

**Lemma 2:** The eigenvalue  $\lambda_k^t$  and the pilot reuse frequency  $n_k^t$  satisfy the relationship:

$$\frac{\sigma^2}{\lambda_k^t} = n_k^t + \frac{\sigma^2}{\lambda_k} \Leftrightarrow n_k^t = \frac{\sigma^2}{\lambda_k^t} - \frac{\sigma^2}{\lambda_k}, \quad k \in \{1, \dots, K\}. \quad (17)$$

*Proof:* Equation (17) holds because the definition of  $n_k^t$  suggests that the  $k$ -th eigenvector is selected by  $n_k^t$  times during timeslots  $1 \sim t$ , so that we have  $\frac{\sigma^2}{\lambda_k^t} = n_k^t + \frac{\sigma^2}{\lambda_k}$ . ■

By comparing **Lemma 2** with the optimal power allocation in (8), we can interpret our proposed ice-filling algorithm as a quantization/solidification version of the water-filling algorithm, which is elaborated below.

**Interpretation of ice-filling:** As depicted in Fig. 4, the water-filling principle allocates  $Q$  units of water (power) to a vessel with  $K$  channels, each having a unique base level  $\frac{\sigma^2}{\lambda_k}$ ,

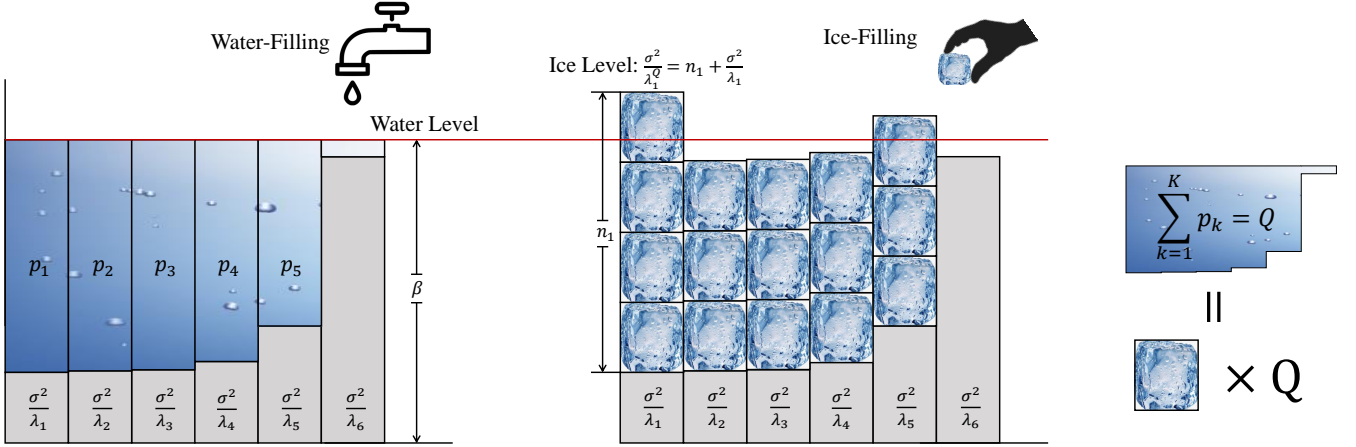


Fig. 4. Comparison between water-filling and ice-filling. The rank of the prior kernel, the number of antennas, and the total pilot length are set as  $K = 6$ ,  $M = 128$ , and  $Q = 16$ , respectively. The eigenvalues of the prior kernel,  $\Sigma_{\mathbf{h}}$ , are in a descending order, i.e.,  $\lambda_1 > \lambda_2 > \lambda_3 > \lambda_4 > \lambda_5 > \lambda_6$ .

$k \in \{1, 2, \dots, K\}$ . By controlling the *uniform* water level  $\beta$ , the optimal power  $p_k$  is determined by the gap between the base level and the water level. In contrast, the ice-filling algorithm transforms the total  $Q$  units of water into  $Q$  ice blocks, each containing one unit of power and being used for one pilot transmission. Our algorithm starts from an empty vessel and fills one ice block onto the channel having the deepest base surface  $\frac{\sigma^2}{\lambda_{k_0}}$ . This operation is equivalent to finding the largest eigenvalue  $\lambda_{k_0}$  from  $\{\lambda_1, \dots, \lambda_K\}$ . Then, the eigenvector  $\mathbf{u}_{k_0}$  is assigned to the first observation vector  $\mathbf{w}_1$ , and ice level of this channel increases from  $\frac{\sigma^2}{\lambda_{k_0}}$  to  $\frac{\sigma^2}{\lambda_{k_0}^2} = \frac{\sigma^2}{\lambda_{k_0}} + 1$ . In the subsequent time slots, the remaining  $Q - 1$  ice blocks are filled onto the channels locating at the deepest base surfaces or ice levels, indexed by  $k_t = \arg \min_k \{\frac{\sigma^2}{\lambda_k^t}\}$ , one by one. The corresponding eigenvectors  $\mathbf{u}_{k_t}$  are used for pilot transmission, and the ice levels increase according to **Lemma 2**. Consequently, the final pilot reuse frequencies  $\{n_k\}$  are determined by the number of ice blocks on top of each channel, and the ice levels are given by  $\{\frac{\sigma^2}{\lambda_k^Q}\} = \{n_k + \frac{\sigma^2}{\lambda_k}\}$ .

The comparison between the ice-filling and water-filling algorithms in Fig. 4 indicates that the continuous powers  $\{p_k\}$  are quantized into the discrete pilot reuse frequencies  $\{n_k\}$  by the ice-filling algorithm. This quantization process naturally results in the non-uniform ice levels  $\{\frac{\sigma^2}{\lambda_k^Q}\}$ , as opposed to the uniform water level  $\beta$  used in the water-filling principle. To further emphasize the quantization nature of ice-filling, we prove **Theorem 2** to upper-bound the quantization error between  $p_k$  and  $n_k$ .

**Theorem 2:** Considering the  $k$ -th pilot reuse frequency,  $n_k$ , and the  $k$ -th optimal power,  $p_k$ , we have

$$|n_k - p_k| < 1. \quad (18)$$

*Proof:* See Appendix C. ■

**Remark 3:** **Theorem 2** rigorously proves that the deviation of  $n_k$  from  $p_k$  is less than 1, rendering the pilot reuse frequency a good approximation of the optimal power allocation. Particularly, when the total pilot length  $Q$  is large, the relative

error between  $n_k$  and  $p_k$  tends to zero because

$$\frac{|n_k - p_k|}{p_k} \leq \frac{1}{p_k} \xrightarrow{Q \rightarrow +\infty} 0. \quad (19)$$

Thereafter, the proposed ice-filling algorithm features a discrete approximation to the ideal water-filling algorithm with the relative quantization error decaying rapidly.

#### D. Majorization Minimization for Phase-Only Controllable Combiner

For dense antenna arrays which can only control their phase shifts, the amplitude of each element of  $\mathbf{W}$  is fixed as a constant. Considering the normalized power constraint, the observation vector at the  $(t + 1)$ -th timeslot can be obtained by

$$\mathbf{w}_{t+1} = \underset{|\mathbf{w}| = \frac{1}{\sqrt{M}} \mathbf{1}_M}{\operatorname{argmax}} \mathbf{w}^H \Sigma_t \mathbf{w}. \quad (20)$$

Due to the unit modulus constraint, the problem (20) is a non-convex programming. To cope with this problem, we propose a MM-based observation matrix design, as presented in **Algorithm 3**. Its key idea is to reformulate the non-convex problem as a series of more tractable approximate subproblems, which can be solved in an alternating manner [47]. Specifically, the proposed MM-based method is illustrated as follows.

To begin with, given that adding a constant to the objective function does not affect the optimal solution of (20), problem (20) is equivalent to

$$\begin{aligned} \mathbf{w}_{t+1} &\stackrel{(a)}{=} \underset{|\mathbf{w}| = \frac{1}{\sqrt{M}} \mathbf{1}_M}{\operatorname{argmax}} \mathbf{w}^H \Sigma_t \mathbf{w} - \lambda_{\max}(\Sigma_t) \mathbf{w}^H \mathbf{w} \\ &= \underset{|\mathbf{w}| = \frac{1}{\sqrt{M}} \mathbf{1}_M}{\operatorname{argmin}} \mathbf{w}^H (\lambda_{\max}(\Sigma_t) \mathbf{I}_M - \Sigma_t) \mathbf{w}, \end{aligned} \quad (21)$$

where (a) holds because  $\mathbf{w}^H \mathbf{w} = 1$ . Then, we consider to solve problem (21) by iteratively minimizing the upper-bound of its objective function. To this end, we introduce an auxiliary variable  $\mathbf{v} \in \mathbb{C}^{M \times 1}$  to obtain an upper-bound function  $\bar{f}(\mathbf{w}, \mathbf{v})$ , given by [48]:

$$\mathbf{w}^H (\lambda_{\max}(\Sigma_t) \mathbf{I}_M - \Sigma_t) \mathbf{w} \leq \bar{f}(\mathbf{w}, \mathbf{v}) =$$

---

**Algorithm 3** MM-Based Observation Matrix Design
 

---

**Input:** Number of pilots  $Q$ , kernel  $\Sigma_{\mathbf{h}}$ .

**Output:** Designed observation matrix  $\mathbf{W}$ .

- 1: Initialization:  $\mathbf{W} = \emptyset$ ,  $\Sigma_0 = \Sigma_{\mathbf{h}}$ .
  - 2: **for**  $t = 0, \dots, Q - 1$  **do**
  - 3:   Initialize  $\mathbf{w}_{t+1}$  randomly
  - 4:   Update:  $\mathbf{X} = \text{Tr}(\lambda_{\max}(\Sigma_t) \mathbf{I}_M - \Sigma_t) \mathbf{I}_M$
  - 5:   **while** no convergence of  $\mathbf{w}_{t+1}^H \Sigma_t \mathbf{w}_{t+1}$  **do**
  - 6:     Update:  $\mathbf{v} = \mathbf{w}_{t+1}$
  - 7:     Update the  $t + 1$ -th observation vector:  $\mathbf{w}_{t+1} = \frac{1}{\sqrt{M}} \exp(j\angle(\mathbf{X} - \lambda_{\max}(\Sigma_t) \mathbf{I}_M + \Sigma_t) \mathbf{v})$
  - 8:   **end while**
  - 9:   Update kernel:  $\Sigma_{t+1} = \Sigma_t - \frac{\Sigma_t \mathbf{w}_{t+1} \mathbf{w}_{t+1}^H \Sigma_t}{\mathbf{w}_{t+1}^H \Sigma_t \mathbf{w}_{t+1} + \sigma^2}$
  - 10: **end for**
  - 11: Construct observation matrix:  $\mathbf{W} = [\mathbf{w}_1, \mathbf{w}_2, \dots, \mathbf{w}_Q]$
  - 12: **return** Designed observation matrix  $\mathbf{W}$
- 

$$\mathbf{w}^H \mathbf{X} \mathbf{w} - 2\Re\{\mathbf{w}^H (\mathbf{X} - \lambda_{\max}(\Sigma_t) \mathbf{I}_M + \Sigma_t) \mathbf{v}\} + \mathbf{v}^H (\mathbf{X} - \lambda_{\max}(\Sigma_t) \mathbf{I}_M + \Sigma_t) \mathbf{v}, \quad (22)$$

where  $\mathbf{X} = \text{Tr}(\lambda_{\max}(\Sigma_t) \mathbf{I}_M - \Sigma_t) \mathbf{I}_M$  and the equality holds when  $\mathbf{v} = \mathbf{w}$ . In this way,  $\mathbf{w}$  and  $\mathbf{v}$  in the upper-bound function  $\tilde{f}(\mathbf{w}, \mathbf{v})$  can be alternatively optimized to approach a sub-optimal solution to problem (21) [47]. In particular, for a given  $\mathbf{w}$ ,  $\mathbf{v}$  can be updated by  $\mathbf{v} = \mathbf{w}$ . For a given  $\mathbf{v}$ , by utilizing  $\mathbf{w}^H \mathbf{X} \mathbf{w} = \text{Tr}(\lambda_{\max}(\Sigma_t) \mathbf{I}_M - \Sigma_t)$  and removing the unrelated part in  $\tilde{f}(\mathbf{w}, \mathbf{v})$  in (22), the subproblem of updating  $\mathbf{w}$  can be rewritten as

$$\mathbf{w}_{t+1} = \underset{|\mathbf{w}| = \frac{1}{\sqrt{M}} \mathbf{1}_M}{\text{argmax}} \Re\{\mathbf{w}^H (\mathbf{X} - \lambda_{\max}(\Sigma_t) \mathbf{I}_M + \Sigma_t) \mathbf{v}\}. \quad (23)$$

It can be easily proved that the optimal solution to (23) is given by  $\mathbf{w}_{t+1} = \frac{1}{\sqrt{M}} \exp(j\angle(\mathbf{X} - \lambda_{\max}(\Sigma_t) \mathbf{I}_M + \Sigma_t) \mathbf{v})$ . This solution, associated with the updating approach of the posterior kernel in **Lemma 1**, completes the algorithm. It is worth noting that, since the updates of  $\mathbf{v}$  and  $\mathbf{w}_{t+1}$  both monotonously increase the objective function, the convergence of **Algorithm 3** is naturally guaranteed.

### E. Kernel Selection in Non-Ideal Case

In practical communication scenarios, obtaining the perfect prior kernel,  $\Sigma_{\mathbf{h}}$ , in the initialization states of **Algorithms 2 and 3** may pose a challenge. To deal with this issue, we suggest two methods to obtain imperfect prior kernels.

1) *Statistical kernel*: Firstly, the prior kernel can be selected as the statistical covariance of historical estimated channels, i.e.,  $\hat{\Sigma}_{\mathbf{h}} = \text{E}(\hat{\mathbf{h}} \hat{\mathbf{h}}^H)$ . Due to the error of channel estimation, the historical channels  $\hat{\mathbf{h}}$  deviate from the true channels  $\mathbf{h}$ . We use a Gaussian noise to model this deviation, and get  $\hat{\mathbf{h}} = \mathbf{h} + \mathbf{z}_{\mathbf{h}}$ , wherein  $\mathbf{z}_{\mathbf{h}} \sim \mathcal{CN}(\mathbf{0}_M, \sigma_{\mathbf{h}}^2 \mathbf{I}_M)$  denotes the historical channel estimation error. For simplicity, we name  $\sigma_{\mathbf{h}}^2$  as the *kernel estimation error*. Thereby, the statistical kernel is modeled as

$$\hat{\Sigma}_{\mathbf{h}} = \Sigma_{\mathbf{h}} + \sigma_{\mathbf{h}}^2 \mathbf{I}_M. \quad (24)$$

2) *Artificial kernels*: Another choice is to employ artificially designed kernels to mimic the perfect kernel. To this end, the artificial kernels should assign high similarity to nearby antennas while diminishing the correlation rapidly with inter-antenna distance. For example, here we consider a general uniform planer array (UPA) equipped with  $M$  antennas with an antenna spacing of  $d$ . The numbers of its horizontal antennas and vertical antennas are  $M_x$  and  $M_y$ , respectively. Striking a balance between complexity and practicality, we recommend two artificial kernels as follows.

- **Exponential kernel**: The exponential kernel  $\Sigma_{\text{exp}}$ , is the most popular selection in Bayesian estimation. Let  $\mathbf{m}_1 = [-\frac{M_1-1}{2}, -\frac{M_1-3}{2}, \dots, \frac{M_1-1}{2}]^T$  and  $\mathbf{m}_2 = [-\frac{M_2-1}{2}, -\frac{M_2-3}{2}, \dots, \frac{M_2-1}{2}]^T$ . Then, the exponential kernels for the two dimensions of UPA,  $\Sigma_{\text{exp},1} \in \mathbb{C}^{M_1 \times M_1}$  and  $\Sigma_{\text{exp},2} \in \mathbb{C}^{M_2 \times M_2}$ , can be respectively expressed as

$$\Sigma_{\text{exp},1} = \exp\left(-\eta_1^2 \frac{4\pi^2 d^2}{\lambda^2} |\mathbf{1}_{M_1}^T \otimes \mathbf{m}_1 - \mathbf{m}_1^T \otimes \mathbf{1}_{M_1}|^{\odot 2}\right), \quad (25)$$

$$\Sigma_{\text{exp},2} = \exp\left(-\eta_1^2 \frac{4\pi^2 d^2}{\lambda^2} |\mathbf{1}_{M_2}^T \otimes \mathbf{m}_2 - \mathbf{m}_2^T \otimes \mathbf{1}_{M_2}|^{\odot 2}\right), \quad (26)$$

where  $\eta_1$  is an adjustable hyper-parameter and  $\mathbf{X}^{\odot 2}$  denotes the element-wise product of two matrices  $\mathbf{X}$ . Then, the overall kernel can be written as

$$\Sigma_{\text{exp}} = \Sigma_{\text{exp},1} \otimes \Sigma_{\text{exp},2}. \quad (27)$$

In comparison to other kernels, the exponential kernel demonstrates lower sensitivity to outliers, rendering it suitable for reconstructing channels lacking obvious regularity.

- **Bessel kernel**: The Bessel kernel, denoted as  $\Sigma_{\text{bes}}$ , is well-suited for capturing and modeling complex-valued data exhibiting oscillatory patterns. The Bessel kernels for the two dimensions of UPA can be expressed as

$$\Sigma_{\text{bes},1} = J_0\left(\eta_2 \frac{2\pi d}{\lambda} |\mathbf{1}_{M_1}^T \otimes \mathbf{m}_1 - \mathbf{m}_1^T \otimes \mathbf{1}_{M_1}|\right), \quad (28)$$

$$\Sigma_{\text{bes},2} = J_0\left(\eta_2 \frac{2\pi d}{\lambda} |\mathbf{1}_{M_2}^T \otimes \mathbf{m}_2 - \mathbf{m}_2^T \otimes \mathbf{1}_{M_2}|\right), \quad (29)$$

where  $J_0$  is the zero-order Bessel function of the first kind and  $\eta_2$  is a hyper-parameter. Thus, the overall kernel can be written as

$$\Sigma_{\text{bes}} = \Sigma_{\text{bes},1} \otimes \Sigma_{\text{bes},2}. \quad (30)$$

$\Sigma_{\text{bes}}$  possesses the flexibility to adapt to data that features regular and repeats fluctuations, which might not be adequately modeled by alternative kernels.

## V. PERFORMANCE ANALYSIS

To evaluate the performance of the proposed MIM-based channel estimators, this section provides comprehensive MSE analyses under different algorithmic conditions.



### A. Estimation Accuracy Under Perfect Kernel

When the perfect prior kernel  $\Sigma_{\mathbf{h}}$  is available, the MSEs achieved by the proposed algorithms can be determined by the trace of their posterior kernels, i.e.,

$$E(\|\mu_{\mathbf{h}|\mathbf{y}} - \mathbf{h}\|_2^2) = \text{Tr}(\Sigma_{\mathbf{h}|\mathbf{y}}). \quad (31)$$

The subsequent two lemmas give out the close-form MSEs and their asymptotic expressions of the water-filling-based and ice-filling-based channel estimators, respectively.

**Lemma 3:** If the perfect kernel  $\Sigma_{\mathbf{h}}$  is adopted, the MSE  $\delta_{\text{wf}}$  of the water-filling algorithm is given by

$$\delta_{\text{wf}} = \sum_{k=1}^K \frac{\lambda_k \sigma^2}{p_k \lambda_k + \sigma^2} \stackrel{Q \rightarrow +\infty}{=} \mathcal{O}(K^2 Q^{-1}). \quad (32)$$

*Proof:* See Appendix D. ■

**Lemma 4:** If the perfect kernel  $\Sigma_{\mathbf{h}}$  is adopted, the MSE  $\delta_{\text{if}}$  of the ice-filling algorithm is given by

$$\delta_{\text{if}} = \sum_{k=1}^K \frac{\lambda_k \sigma^2}{n_k \lambda_k + \sigma^2} \stackrel{Q \rightarrow +\infty}{=} \mathcal{O}(K^2 Q^{-1}). \quad (33)$$

*Proof:* See Appendix E. ■

We can gain two insights from **Lemma 3** and **Lemma 4**. Firstly, the MSEs achieved by **Algorithm 1** and **Algorithm 2** have identical asymptotic expressions, both of which decay at the rate of  $Q^{-1}$ . The only difference is owing to the quantization of the continuous powers  $\{p_k\}$  in (32) to the pilot reuse frequencies  $\{n_k\}$  in (33). Next, the MSEs decay quadratically as the rank of the channel kernel,  $K$ , decreases. This finding demonstrates the superiority of DASs in channel estimation. A denser antenna deployment increases the correlation between inter-antenna channels, decreases the rank of the channel kernel, and thereby improves the channel estimation accuracy.

Taking into account the quantization nature revealed in **Theorem 2**, the asymptotic achievability bound of the MSE of the ice-filling algorithm can be evaluated by the following theorem.

**Theorem 3:** As  $Q \rightarrow +\infty$ , the asymptotic MSE difference,  $|\delta_{\text{wf}} - \delta_{\text{if}}|$ , is given by

$$|\delta_{\text{wf}} - \delta_{\text{if}}| = \mathcal{O}(K^3 Q^{-2}). \quad (34)$$

*Proof:* See Appendix F. ■

**Remark 4:** *Theorem 3* guarantees that the MSE gap between the ice-filling and the ideal water-filling algorithms decays at a rate of  $K^3 Q^{-2}$ , which demonstrates the near-optimality of the proposed ice-filling channel estimator when  $Q \rightarrow +\infty$  or  $K \rightarrow 0$ .

To validate the superiority of the proposed design, it is of great interest to evaluate the MSE achieved by the Bayesian regression (5) using randomly generated observation matrices. For amplitude-and-phase controllable cases, we assume that all elements of  $\mathbf{W}$  are independently generated from a Gaussian distribution  $\mathcal{CN}(0, 1/M)$ . For phase-only controllable cases, the angles of all elements of  $\mathbf{W}$  are randomly selected from  $[-\pi, +\pi]$ . Then, we derive the asymptotic MSE of a random observation matrix in **Lemma 5**.

**Lemma 5:** Assume that the perfect kernel  $\Sigma_{\mathbf{h}}$  is adopted and  $Q$  is sufficiently large. When  $\mathbf{W}$  is randomly generated, the MSE  $\delta_{\text{rnd}}$  achieved in both phase-and-amplitude and phase-only controllable cases can be approximated by

$$\delta_{\text{rnd}} \approx \sum_{k=1}^K \frac{\lambda_k \sigma^2}{\frac{Q}{M} \lambda_k + \sigma^2} \stackrel{Q \rightarrow +\infty}{=} \mathcal{O}(KMQ^{-1}), \quad (35)$$

where the approximate equality can be infinitely close to an equality as  $Q \rightarrow \infty$ .

*Proof:* See Appendix G. ■

It is evident from **Lemmas 3-5** that meticulously designed observation matrices can scale down the asymptotic MSE from  $\mathcal{O}(KMQ^{-1})$  to  $\mathcal{O}(K^2 Q^{-1})$ . This improvement is attributed to the fact that the observation matrices designed by water-filling and ice-filling approaches are tightly aligned with the kernel's eigenspace of dimension  $K$ . In contrast, the random observation matrix wastes a large amount of power in the kernel's null space of dimension  $M - K$ , which contains no useful information about the channel. This finding demonstrates the significant role played by the observation matrix to enhance channel estimation accuracy, particularly in DASs where  $M \gg K$ .

### B. Estimation Accuracy Under Imperfect Kernel

We now consider the situation where the perfect prior kernel  $\Sigma_{\mathbf{h}}$  is not available. In this context, an imperfect prior kernel, such as the statistical kernel in (24) and the artificial kernels (27) and (30), has to be adopted in the proposed algorithms. We denote the adopted prior kernel as  $\Sigma$ . Then, one can use the following lemma to evaluate the MSE performance analytically.

**Lemma 6:** Given a prior kernel  $\Sigma$  as the input of the proposed channel estimator, the MSE  $\hat{\delta}$  of channel estimation is given by

$$\hat{\delta} = \text{Tr}((\mathbf{\Pi}^H \mathbf{W}^H - \mathbf{I}_M) \Sigma_{\mathbf{h}} (\mathbf{W} \mathbf{\Pi} - \mathbf{I}_M)) + \sigma^2 \text{Tr}(\mathbf{\Pi}^H \mathbf{\Pi}), \quad (36)$$

where  $\mathbf{\Pi} := (\mathbf{W}^H \Sigma \mathbf{W} + \sigma^2 \mathbf{I}_Q)^{-1} \mathbf{W}^H \Sigma$ .

*Proof:* See Appendix H. ■

**Lemma 6** indicates that, the estimation error caused by the non-ideal input cannot be neglected. For example, if the input kernel  $\Sigma$  behaves far from the real kernel  $\Sigma_{\mathbf{h}}$ , the value of the MSE may become significantly large due to the existence of  $\mathbf{\Pi}$  in (36). In this case, one may be concerned about the optimality and the accessibility of the proposed estimator when  $\Sigma$  can be arbitrarily selected. To answer the question, we derive the following corollary.

**Corollary 1:** The lower-bound of the achievable MSE  $\hat{\delta}$  is exactly the trace of posterior covariance  $\Sigma_{\mathbf{h}|\mathbf{y}}$  under perfect kernel, i.e.,  $\min_{\Sigma} \hat{\delta} = \text{Tr}(\Sigma_{\mathbf{h}|\mathbf{y}})$ , which is achieved if and only if the input kernel satisfies  $\Sigma = \Sigma_{\mathbf{h}}$ .

*Proof:* See Appendix I. ■

Coinciding with the well-known linear estimation theory, the above corollary is proved from the other perspective, and suggests that the real kernel is actually the best prior knowledge for Bayesian regression. It also reveals the equivalence

between a kernel-based Bayesian reconstructor and a classical MMSE estimator in DAS channel estimation.

To obtain more insightful results, we use the statistical kernel,  $\hat{\Sigma}_{\mathbf{h}}$  in (24), as an example to analyze the achievable MSEs. To ease the derivation, we first prove a useful expression of the MSE in **Lemma 7**.

**Lemma 7:** The MSE  $\hat{\delta}$  in (36) under the imperfect kernel  $\hat{\Sigma}_{\mathbf{h}}$  can be written as a function of  $\mathbf{W}\mathbf{W}^H$ , given by

$$\begin{aligned} \hat{\delta} = & \text{Tr} \left( \left( \hat{\Sigma}_{\mathbf{h}}^H \Omega^H - \mathbf{I}_M \right) \Sigma_{\mathbf{h}} \left( \Omega \hat{\Sigma}_{\mathbf{h}} - \mathbf{I}_M \right) \right) \\ & + \sigma^2 \text{Tr} \left( \hat{\Sigma}_{\mathbf{h}} \Xi \hat{\Sigma}_{\mathbf{h}} \right), \end{aligned} \quad (37)$$

wherein  $\Omega$  and  $\Xi$  are subfunctions of  $\mathbf{W}\mathbf{W}^H$ , written as

$$\begin{aligned} \Omega &= \frac{\mathbf{W}\mathbf{W}^H}{\sigma^2} - \frac{\mathbf{W}\mathbf{W}^H}{\sigma^4} \left( \hat{\Sigma}_{\mathbf{h}}^{-1} + \frac{\mathbf{W}\mathbf{W}^H}{\sigma^2} \right)^{-1} \mathbf{W}\mathbf{W}^H, \quad (38) \\ \Xi &= \frac{\mathbf{W}\mathbf{W}^H}{\sigma^4} - 2 \frac{\mathbf{W}\mathbf{W}^H}{\sigma^6} \left( \hat{\Sigma}_{\mathbf{h}}^{-1} + \frac{\mathbf{W}\mathbf{W}^H}{\sigma^2} \right)^{-1} \mathbf{W}\mathbf{W}^H + \\ & \frac{\mathbf{W}\mathbf{W}^H}{\sigma^8} \left( \left( \hat{\Sigma}_{\mathbf{h}}^{-1} + \frac{\mathbf{W}\mathbf{W}^H}{\sigma^2} \right)^{-1} \mathbf{W}\mathbf{W}^H \right)^2. \quad (39) \end{aligned}$$

*Proof:* See Appendix J. ■

Recall that the essential difference among the three estimators, i.e., water-filling algorithm, ice-filling algorithm, and the estimator with randomly generated  $\mathbf{W}$ , is the form of observation matrix  $\mathbf{W}$ . Thus, by utilizing **Lemma 7**, the MSE of different algorithms under the imperfect kernel  $\hat{\Sigma}_{\mathbf{h}}$  can be obtained by replacing  $\mathbf{W}\mathbf{W}^H$  in  $\hat{\delta}$  with their corresponding analytical expressions. Aided by some matrix operations, we can thereby prove the following lemma.

**Lemma 8:** Under the imperfect kernel  $\hat{\Sigma}_{\mathbf{h}}$ , the achievable MSE for the water-filling algorithm can be written as

$$\begin{aligned} \hat{\delta}_{\text{wf}} = & \sigma^2 \sum_{k=1}^K \frac{\lambda_k \sigma^2 + \hat{p}_k (\lambda_k + \sigma_{\mathbf{h}}^2)^2}{(\hat{p}_k (\lambda_k + \sigma_{\mathbf{h}}^2) + \sigma^2)^2} + \sigma^2 \sum_{m=K+1}^M \frac{\hat{p}_m \sigma_{\mathbf{h}}^4}{(\hat{p}_m \sigma_{\mathbf{h}}^2 + \sigma^2)^2} \\ & \stackrel{Q \rightarrow +\infty}{=} \mathcal{O}(\sigma^2 M^2 Q^{-1}), \end{aligned} \quad (40)$$

wherein  $\{\lambda_1, \dots, \lambda_M\}$  represent the  $M$  non-negative eigenvalues of  $\Sigma_{\mathbf{h}}$  in a descending order<sup>1</sup>. The power  $\hat{p}_m$  allocated to each eigenvector is calculated by the water-filling principle  $\hat{p}_m = \left( \hat{\beta} - \frac{\sigma^2}{\lambda_m + \sigma_{\mathbf{h}}^2} \right)^+$  for  $m \in \{1, \dots, M\}$ . The water-level  $\hat{\beta}$  can be determined via binary search such that  $\sum_{m=1}^M \hat{p}_m = Q$ .

Under the imperfect kernel  $\hat{\Sigma}_{\mathbf{h}}$ , the achievable MSE for the ice-filling algorithm can be written as

$$\begin{aligned} \hat{\delta}_{\text{if}} = & \sigma^2 \sum_{k=1}^K \frac{\lambda_k \sigma^2 + \hat{n}_k (\lambda_k + \sigma_{\mathbf{h}}^2)^2}{(\hat{n}_k (\lambda_k + \sigma_{\mathbf{h}}^2) + \sigma^2)^2} + \sigma^2 \sum_{m=K+1}^M \frac{\hat{n}_m \sigma_{\mathbf{h}}^4}{(\hat{n}_m \sigma_{\mathbf{h}}^2 + \sigma^2)^2} \\ & \stackrel{Q \rightarrow +\infty}{=} \mathcal{O}(\sigma^2 M^2 Q^{-1}), \end{aligned} \quad (41)$$

wherein the pilot reuse frequencies  $\{\hat{n}_1, \dots, \hat{n}_M\}$  can be obtained by **Algorithm 2** with  $\hat{\Sigma}_{\mathbf{h}}$  being the input kernel. In particular,  $\sum_{m=1}^M \hat{n}_m = Q$  holds.

For the estimator enabled by a randomly generated  $\mathbf{W}$  with sufficiently large  $Q$ , the achievable MSE under the imperfect kernel  $\hat{\Sigma}_{\mathbf{h}}$  can be written as

$$\begin{aligned} \hat{\delta}_{\text{rnd}} \approx & \sigma^2 \sum_{k=1}^K \frac{\lambda_k \sigma^2 + \frac{Q}{M} (\lambda_k + \sigma_{\mathbf{h}}^2)^2}{\left( \frac{Q}{M} (\lambda_k + \sigma_{\mathbf{h}}^2) + \sigma^2 \right)^2} + \sigma^2 \sum_{m=K+1}^M \frac{\frac{Q}{M} \sigma_{\mathbf{h}}^4}{\left( \frac{Q}{M} \sigma_{\mathbf{h}}^2 + \sigma^2 \right)^2} \\ & \stackrel{Q \rightarrow +\infty}{=} \mathcal{O}(\sigma^2 M^2 Q^{-1}), \end{aligned} \quad (42)$$

wherein the approximate equality can be infinitely close to an equality as  $Q \rightarrow \infty$ .

*Proof:* See Appendix K. ■

From **Lemma 8**, it is easy to prove that the MSEs under the imperfect kernel  $\hat{\Sigma}_{\mathbf{h}}$  are increased by the kernel estimation error  $\sigma_{\mathbf{h}}^2$ . The reason is that, the estimation error makes the input kernel full-rank, i.e.,  $\hat{\Sigma}_{\mathbf{h}} = \Sigma_{\mathbf{h}} + \sigma_{\mathbf{h}}^2 \mathbf{I}_M$ . Then, the power (or pilot reuse frequency) for estimation may be allocated to all eigenvectors of  $\Sigma_{\mathbf{h}}$ . However, allocating power to those eigenvectors associated with the eigenvalue  $\sigma_{\mathbf{h}}^2$  contributes nearly no improvement to channel recovery accuracy. Besides, an imperfect kernel input also changes the weights of the posterior mean  $\mu_{\mathbf{h}|\mathbf{y}}$  in (5), which resembles a Bayesian estimator that underestimates the impact of noise.

**Remark 5:** According to (40), (41), and (42), an efficient way to alleviate the effect of  $\sigma_{\mathbf{h}}^2$  on MSEs is to introduce the prior knowledge that the real kernel  $\Sigma_{\mathbf{h}}$  is rank- $K$ . Then, the estimator only allocates power to the eigenvalues associated with the  $K$ -largest eigenvalues of  $\hat{\Sigma}_{\mathbf{h}}$ , so that the second term in (40), (41), and (42) can be eliminated. For example, when  $p_m$  for  $m > K$  are forced to be zero,  $\hat{\delta}_{\text{wf}}$  in (40) becomes

$$\begin{aligned} \hat{\delta}_{\text{wf}} = & \sigma^2 \sum_{k=1}^K \frac{\lambda_k \sigma^2 + p_k (\lambda_k + \sigma_{\mathbf{h}}^2)^2}{(p_k (\lambda_k + \sigma_{\mathbf{h}}^2) + \sigma^2)^2} \\ & \stackrel{Q \rightarrow +\infty}{=} \mathcal{O}(\sigma^2 K^2 Q^{-1}), \end{aligned} \quad (43)$$

wherein  $p_k$  for  $k \in \{1, \dots, K\}$  is given in (8). For  $\sigma_{\mathbf{h}}^2 > 0$ , it is evident that  $\hat{\delta}_{\text{wf}}$  in (43) is lower than that in (40).

Based on the results in **Lemma 8**, the asymptotic MSEs when the kernel estimation error  $\sigma_{\mathbf{h}}^2$  is infinitely large are expressed as follows.

**Corollary 2:** When  $\sigma_{\mathbf{h}}^2 \rightarrow +\infty$ , the asymptotic MSEs  $\hat{\delta}$  for the water-filling algorithm, ice-filling algorithm, and the estimator based on random  $\mathbf{W}$  can be respectively written as

$$\hat{\delta}_{\text{wf}} \stackrel{\sigma_{\mathbf{h}}^2 \rightarrow +\infty}{=} \mathcal{O} \left( \sigma^2 \sum_{k=1}^{L_{\text{wf}}} \hat{p}_k^{-1} \right) = \mathcal{O}(\sigma^2 M^2 Q^{-1}), \quad (44)$$

$$\hat{\delta}_{\text{if}} \stackrel{\sigma_{\mathbf{h}}^2 \rightarrow +\infty}{=} \mathcal{O} \left( \sigma^2 \sum_{k=1}^{L_{\text{if}}} \hat{n}_k^{-1} \right) = \mathcal{O}(\sigma^2 M^2 Q^{-1}), \quad (45)$$

$$\hat{\delta}_{\text{rnd}} \stackrel{\sigma_{\mathbf{h}}^2 \rightarrow +\infty}{=} \mathcal{O}(\sigma^2 M^2 Q^{-1}), \quad (46)$$

where  $L_{\text{wf}}$  and  $L_{\text{if}}$  are the numbers of the positive values in  $\{\hat{p}_m\}_{m=1}^M$  and  $\{\hat{n}_m\}_{m=1}^M$ , respectively.

*Proof:* The three asymptotic MSEs can be easily obtained by letting  $\sigma_{\mathbf{h}}^2 \rightarrow +\infty$  for  $\hat{\delta}_{\text{wf}}$  in (40),  $\hat{\delta}_{\text{if}}$  in (41), and  $\hat{\delta}_{\text{rnd}}$  in (42), respectively. Since their derivations are similar, here we focus on the asymptotic  $\hat{\delta}_{\text{wf}}$  as an example. By letting  $\sigma_{\mathbf{h}}^2 \rightarrow +\infty$  and removing the small-order components, we have

<sup>1</sup>That is to say, if  $\Sigma_{\mathbf{h}}$  is rank- $K$ , we have  $\lambda_m = 0$  for all  $m > K$ .

TABLE I  
SIMULATION PARAMETERS OF CHANNEL MODEL IN 3GPP TR 38.901

Channel parameters	Values in [49]
Carrier frequency $f_c$	3.5 GHz
Number of clusters	23
Number of rays per cluster	20
Path gains	$\mathcal{CN}(0, 1)$
Incident angles	$\mathcal{U}(-90^\circ, +90^\circ)$
Maximum angle spread	$\mathcal{U}(-5^\circ, +5^\circ)$
Maximum delay spread	$\mathcal{U}(-30 \text{ ns}, +30 \text{ ns})$

$\hat{\delta}_{\text{wof}} \stackrel{\sigma_{\mathbf{h}}^2 \rightarrow +\infty}{=} \mathcal{O}\left(\sigma^2 \sum_{k=1}^{L_{\text{wof}}} \hat{p}_k^{-1}\right)$ . Since  $\hat{p}_m = \left(\hat{\beta} - \frac{\sigma^2}{\lambda_m + \sigma_{\mathbf{h}}^2}\right)^+$  for  $m \in \{1, \dots, M\}$ , we have  $\hat{p}_m = \hat{\beta} = \frac{Q}{M}$  and  $L_{\text{wof}} = M$ , which completes the proof. ■

### C. Computational Complexity Analysis

The computational complexity of the proposed channel estimators is low in practical applications. Specifically, according to Fig. 3, the computational complexity can be divided into two components, i.e., observation matrix design in Stage 1 and Bayesian regression in Stage 2.

For the observation matrix design, the complexity of **Algorithm 1** is mainly caused by the eigenvalue decomposition and matrix reconstruction, which is  $\mathcal{O}(M^3 + MKQ)$ . The complexity of **Algorithm 2** is mainly caused by the eigenvalue decomposition and the principal eigenvalue selection, which is  $\mathcal{O}(M^3 + QK)$ . The complexity of **Algorithm 3** mainly depends on the search for the largest eigenvalue and the iterations required for the convergence of MM, which is  $\mathcal{O}(M^3 + I_o M^2 Q)$  wherein  $I_o$  is the number of iterations. and then saved in the memory medium in advance.

For the Bayesian regression, according to (5), we find that the recovered channel  $\hat{\mathbf{h}}$  is exactly the weighted sum of received pilots  $\mathbf{y}$ . In particular, the weight is calculated by  $\Sigma_{\mathbf{h}} \mathbf{W} (\mathbf{W}^H \Sigma_{\mathbf{h}} \mathbf{W} + \sigma^2 \mathbf{I}_Q)^{-1}$ , thus the overall complexity of Stage 2 is  $\mathcal{O}(M^3)$ . It is notable that the weight only relies on the designed  $\mathbf{W}$  and  $\Sigma_{\mathbf{h}}$ . It means that the weight for recovering  $\mathbf{h}$  can also be calculated offline and then employed for online channel estimation.

## VI. SIMULATION RESULTS

In this section, we present simulation results to verify the effectiveness of the proposed channel estimators for DASs.

### A. Simulation Setup and Benchmarks

To account for a practical scenario, the standard 3GPP TR 38.901 channel model is used for simulations, whose key parameters are given in Table I. Otherwise specifically specified, we consider a UPA. The number of antennas is set to  $M = 128$ , and the numbers of horizontal antennas and vertical antennas are set to  $M_x = 16$  and  $M_y = 8$ , respectively. Assume that the antenna spacing is set to  $\frac{\lambda}{8}$ . The

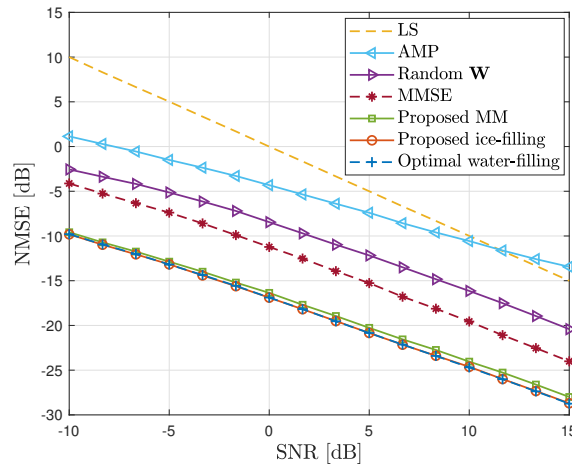


Fig. 5. The effect of SNR on NMSE performance under perfect kernel  $\Sigma_{\mathbf{h}}$ .

signal-to-noise ratio (SNR) is defined as  $\text{SNR} = \frac{E(\|\mathbf{h}\|^2)}{\sigma^2}$ , of which the default value is set to 10 dB. Let  $\hat{\mathbf{h}}$  denote the estimated value of channel  $\mathbf{h}$ . The performance is evaluated by the normalized mean square error (NMSE), which is defined as  $\text{NMSE} = E\left(\frac{\|\mathbf{h} - \hat{\mathbf{h}}\|^2}{\|\mathbf{h}\|^2}\right)$ . Besides, 3000 Monte-Carlo experiments are carried out to plot each figure.

To demonstrate the effectiveness of the proposed ice-filling and MM enabled channel estimators, seven channel estimation schemes are considered for comparison:

- **LS**: The classic LS method is applicable when the pilot length is no less than the number of antennas. To implement it, the observation matrix,  $\mathbf{W}$ , is set to a DFT matrix.
- **MMSE**: Setting the observation matrix as the DFT matrix, the classic MMSE method is harnessed to recover the channel by using the Bayesian regression in (5).
- **AMP**: The vectored approximate message passing (AMP) method proposed in [32] is leveraged to estimate the sparse channel in angular domain.
- **Optimal water-filling**: The water-filling scheme in **Algorithm 1** is employed to design the ideal observation matrix  $\mathbf{W}$ . Based on  $\mathbf{W}$ , the Bayesian regression in (5) is performed, which serves as the lower bound of NMSE.
- **Random W**: An observation matrix  $\mathbf{W}$  of  $Q$ -pilot length is randomly generated with standard complex Gaussian distribution and utilized for Bayesian regression.
- **Proposed ice-filling**: The ice-filling scheme in **Algorithm 2** is employed to design the observation matrix  $\mathbf{W}$ . Then,  $\mathbf{W}$  is used for Bayesian regression in (5).
- **Proposed MM**: The MM-based scheme in **Algorithm 3** is employed to design the observation matrix  $\mathbf{W}$ . Then,  $\mathbf{W}$  is used for Bayesian regression in (5).

Note that the pilot length for the LS and MMSE methods is  $Q = M = 128$ , while that for the other schemes is set to  $Q = 64$  by default.

### B. Performance Evaluation Under Perfect Kernel

In this subsection, we use the perfect kernel,  $\Sigma_{\mathbf{h}}$ , to trigger the water-filling, ice-filling, and MM algorithms, and then

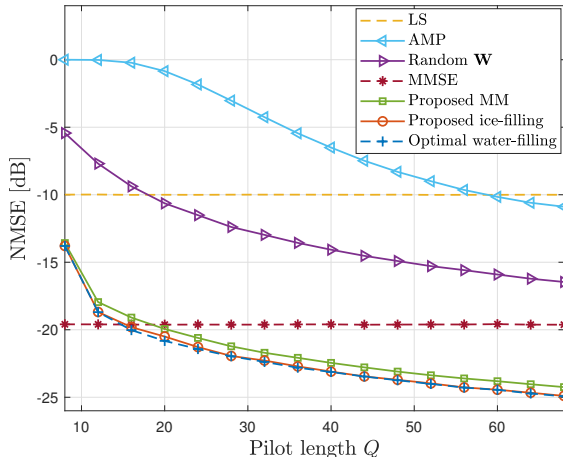


Fig. 6. The NMSE as a function of pilot length. The pilot length allocated to the LS and MMSE methods is fixed to 128, whereas the pilot length  $Q$  for other schemes rises from 8 to 68.

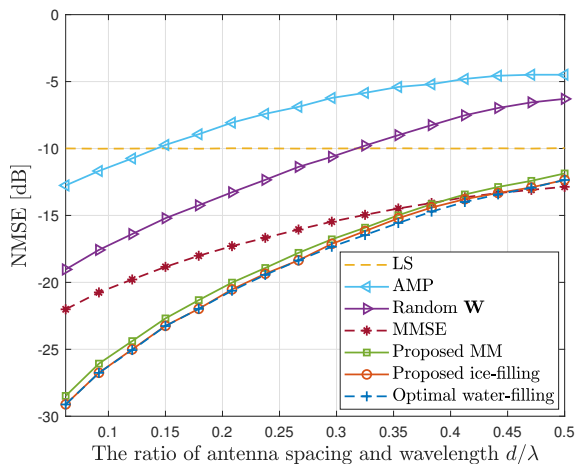


Fig. 7. NMSE versus the ratio of antenna spacing and wavelength.

perform the Bayesian regression. The NMSE performance as a function of SNR is evaluated in Fig. 5. The SNR ranges from  $-10$  dB  $\sim$   $15$  dB. Thanks to the careful design of observation matrix, the optimal water-filling, the proposed ice-filling, and the proposed MM algorithms remarkably outperform existing benchmarks. In particular, a 5 dB NMSE gap between ice-filling and MMSE, as well as a 15 dB gap between ice-filling and AMP, are visible when the SNR is 10 dB. Notably, the NMSE performance attained by the ice-filling method tightly aligns with that of the ideal water-filling scheme, given that the ice-filling intrinsically allocates  $Q$  quantized units of power to the  $Q$ -timeslot pilots. Another finding of interest is that the NMSE gap between the MM and ice-filling algorithms is no higher than 1 dB, demonstrating the near-optimality of the proposed MM algorithm in phase-only-controllable design.

Next, we investigate the impact of pilot length,  $Q$ , on the NMSE performance in Fig. 6. The pilot length allocated to the LS and MMSE methods is fixed to 128, whereas the pilot length for the other algorithms ranges from 8 to 68. It is evident from Fig. 6 that the proposed algorithms consume significantly lower pilot overhead than the other benchmarks

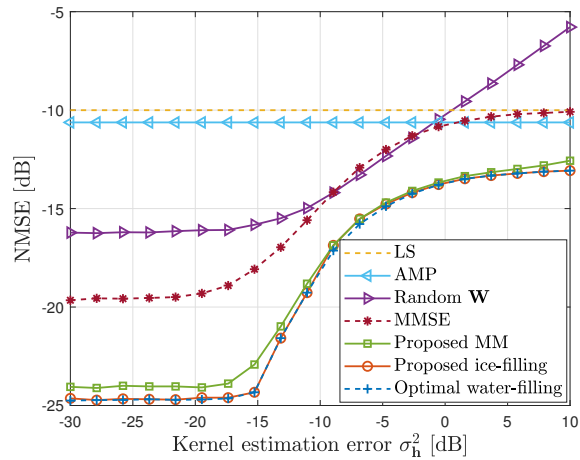


Fig. 8. The effect of kernel estimation error on NMSE performance under the imperfect kernel  $\hat{\Sigma}_h$ .

to achieve the same NMSE level. For instance, to obtain a  $-15$  dB NMSE, the pilot lengths required for the random observation matrix design and the AMP algorithm are larger than 48 and 68, respectively. In contrast, to reach the same NMSE level, a 10-timeslot pilot transmission is sufficient for the proposed ice-filling and MM algorithms. Thereby, we can conclude that, our proposed schemes are capable of saving approximately 80% of pilot overhead. Additionally, it is notable that when the pilot length is around 20, the optimal water-filling algorithm slightly outperforms the ice-filling algorithm due to the power quantization. This observation validates that the optimal water-filling is a performance upper bound of our practical design.

In Fig. 7, we demonstrate the superiority of a DAS in precise channel estimation. The curves of the achieved NMSE performance versus the ratio of antenna spacing and wavelength, i.e.,  $\frac{d}{\lambda}$ , are plotted. We can observe that, as the normalized antenna spacing  $\frac{d}{\lambda}$  decreases from  $\frac{1}{2}$  to  $\frac{1}{16}$ , the NMSEs for all channel estimators excluding LS method declines rapidly. For example, the NMSE achieved by the proposed ice-filling algorithm is decreased by about 10 dB when the antenna spacing ranges from  $\lambda/2$  to  $\lambda/8$ . This phenomenon is attributed to the fact that, a smaller antenna spacing leads to stronger spatial correlations of channels over different antennas, which results in a more informative kernel  $\Sigma_h$  for more precise channel reconstruction. Since the underpinning spatial information of wireless channels is embedded in the structured kernel, these Bayesian optimization based channel estimators are enhanced under DASs.

### C. Performance Evaluation Under Imperfect Kernel

In some scenarios where the perfect prior kernel  $\Sigma_h$  cannot be obtained, the statistical kernel and artificial kernels defined in Section IV-E can be utilized to replace the perfect kernel  $\Sigma_h$  in Algorithms 1~3. We first consider the statistical kernel  $\hat{\Sigma}_h = \Sigma_h + \sigma_h^2 \mathbf{I}_M$ . The NMSE as a function of the kernel estimation error  $\sigma_h^2$  is shown in Fig. 8. One can observe that all kernel-dependent methods, including the MMSE, Random  $\mathbf{W}$ , and the proposed estimators, suffer from visible perfor-

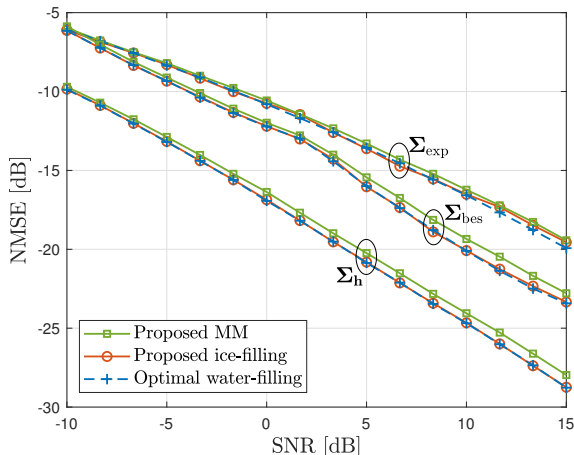


Fig. 9. The effect of SNR on NMSE performance under the perfect kernel  $\Sigma_{\mathbf{h}}$ , the Bessel kernel  $\Sigma_{\text{bes}}$ , and the exponential kernel  $\Sigma_{\text{exp}}$ .

mance loss due to the imperfect kernel input. Fortunately, the proposed methods still hold the superiority among all schemes. In particular, the estimation accuracy of the proposed methods is almost not influenced when  $\sigma_{\mathbf{h}}^2 < -15$  dB, which shows their high robustness to the kernel error. One more interesting finding is that, when  $\sigma_{\mathbf{h}}^2$  increases, the gap between MMSE and our proposed methods, become small. The reason is that, an increasing  $\sigma_{\mathbf{h}}^2$  gradually obscures the structural characteristics of  $\Sigma_{\mathbf{h}}$ , which makes the input kernel  $\hat{\Sigma}_{\mathbf{h}}$  behaves more like an identity matrix. In this case, the importance of designing the observation matrix  $\mathbf{W}$  is reduced.

We further evaluate the achievable NMSE performance under the artificial kernels  $\Sigma_{\text{exp}}$  and  $\Sigma_{\text{Bes}}$ . Their hyper-parameters,  $\eta_1$  and  $\eta_2$ , are determined by the binary search through several numerical experiments, which are set to  $\eta_1 = 0.56$  and  $\eta_2 = 0.85$  in the considered scenario. In this way, we obtain the NMSE versus the SNR and that versus the pilot length  $Q$  in Fig. 9 and Fig. 10, respectively. From these two figures one find that, for a given kernel, the curves of “optimal water-filling”, “proposed ice-filling”, and “proposed MM” are very close, which indicates that these three schemes have similar robustness to imperfect kernels. This phenomenon proves the feasibility of using experiential kernels.

More importantly, one can find that the imperfect kernels lead to a decrease in estimation performances, while the CSI accuracy still holds considerable. Compared with the NMSE achieved by the perfect kernel, those achieved by the imperfect kernels experience an increase of about 5 dB. For example, when the SNR is set to 5 dB, the NMSEs of the proposed estimators for kernels  $\Sigma_{\mathbf{h}}$ ,  $\Sigma_{\text{Bes}}$ , and  $\Sigma_{\text{exp}}$  are about  $-20$  dB,  $-15$  dB, and  $-13$  dB, respectively. To achieve the NMSE of  $-15$  dB, the required pilot lengths  $Q$  for the three kernels are 12, 20, and 24, respectively. Despite the performance losses, we find that the superiority of the proposed methods still hold while comparing to the baselines in Fig. 5 and Fig. 6. This observation is encouraging because it suggests that the proposed methods may not require real prior knowledge of channels. As an alternative, a virtual kernel composed of experiential parameters may be an ideal choice in practice,

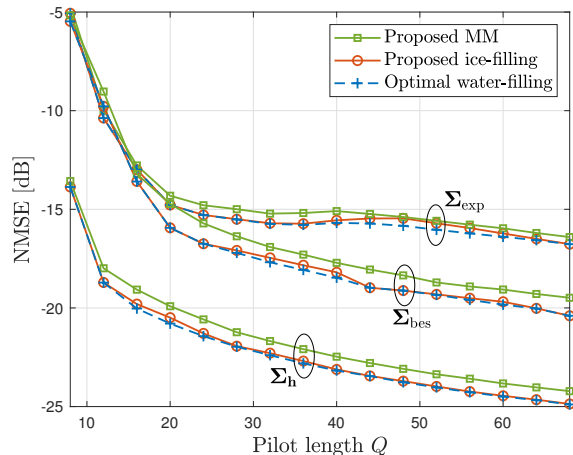


Fig. 10. The effect of pilot length on NMSE performance under the perfect kernel  $\Sigma_{\mathbf{h}}$ , the Bessel kernel  $\Sigma_{\text{bes}}$ , and the exponential kernel  $\Sigma_{\text{exp}}$ .

such that gains without pain can be achieved.

## VII. CONCLUSIONS

This paper incorporated the design of observation matrix into Bayesian channel estimation in DASs. The formulated MIM-based observation matrix design was shown to be a time-domain duality of classic MIMO precoding, which was ideally addressed by the water-filling principle. Targeting practical DAS realizations, we proposed a novel ice-filling and a MM enabled algorithms to design amplitude-and-phase controllable and phase-only controllable observation matrices, respectively. In particular, the ice-filling algorithm was proved to be a discrete approximation of water-filling, with the relative quantization error decaying rapidly. Comprehensive analyses on the MSEs of channel estimation and their asymptotic expressions validated the near-optimality of the proposed designs. Last, numerical results illustrated that our algorithms could improve the channel estimation accuracy by orders of magnitude.

This work establishes a new understanding of channel estimation from the view of information theory. Several potential directions for extending our work are summarized as follows. In current communication systems, beam selection techniques, including beam training and beam tracking, are widely adopted CSI acquisition approaches. Designing new beam selection strategies using the idea of MIM will be interesting. Besides, the extension to more general systems, such as multi-user MIMO and wideband communications, and theoretically analyzing their channel estimation accuracy also deserve in-depth study.

## APPENDIX A

### DERIVATION OF $I(\mathbf{y}_{t+1}; \mathbf{h}) - I(\mathbf{y}_t; \mathbf{h})$

The MI  $I(\mathbf{y}_{t+1}; \mathbf{h})$  can be decoupled as

$$\begin{aligned} I(\mathbf{y}_{t+1}; \mathbf{h}) &= \log_2 \left| \mathbf{I}_{t+1} + \frac{1}{\sigma^2} \mathbf{W}_{t+1}^H \Sigma_{\mathbf{h}} \mathbf{W}_{t+1} \right| \\ &= \log_2 \left| \begin{array}{cc} \mathbf{I}_t + \frac{1}{\sigma^2} \mathbf{W}_t^H \Sigma_{\mathbf{h}} \mathbf{W}_t & \frac{1}{\sigma^2} \mathbf{W}_t^H \Sigma_{\mathbf{h}} \mathbf{w}_{t+1} \\ \frac{1}{\sigma^2} \mathbf{w}_{t+1}^H \Sigma_{\mathbf{h}} \mathbf{W}_t & 1 + \frac{1}{\sigma^2} \mathbf{w}_{t+1}^H \Sigma_{\mathbf{h}} \mathbf{w}_{t+1} \end{array} \right| \end{aligned}$$

$$\stackrel{(a)}{=} \log_2 \left| \begin{array}{cc} \mathbf{I}_t + \frac{1}{\sigma^2} \mathbf{W}_t^H \Sigma_{\mathbf{h}} \mathbf{W}_t & \frac{1}{\sigma^2} \mathbf{W}_t^H \Sigma_{\mathbf{h}} \mathbf{w}_{t+1} \\ \mathbf{0} & 1 + \frac{1}{\sigma^2} \mathbf{w}_{t+1}^H \Sigma_t \mathbf{w}_{t+1} \end{array} \right|$$

$$= I(\mathbf{y}_t; \mathbf{h}) + \log_2 \left( 1 + \frac{1}{\sigma^2} \mathbf{w}_{t+1}^H \Sigma_t \mathbf{w}_{t+1} \right), \quad (47)$$

where (a) holds because of the relationship in (48). Clearly,  $I(\mathbf{y}_{t+1}; \mathbf{h}) - I(\mathbf{y}_t; \mathbf{h})$  is  $\log_2 \left( 1 + \frac{1}{\sigma^2} \mathbf{w}_{t+1}^H \Sigma_t \mathbf{w}_{t+1} \right)$ .

#### APPENDIX B PROOF OF LEMMA 1

The key to this proof lies in calculating the inverse of  $\mathbf{W}_t^H \Sigma_{\mathbf{h}} \mathbf{W}_t + \sigma^2 \mathbf{I}_t$  in (10). For ease of notation, we denote  $\mathbf{K}_t = \mathbf{W}_t^H \Sigma_{\mathbf{h}} \mathbf{W}_t + \sigma^2 \mathbf{I}_t$  and  $\mathbf{W}_t = [\mathbf{W}_{t-1}, \mathbf{w}_t]$ . Then  $\mathbf{K}_t$  can be expressed in a block matrix form:

$$\mathbf{K}_t = \begin{bmatrix} \mathbf{W}_{t-1}^H \Sigma_{\mathbf{h}} \mathbf{W}_{t-1} + \sigma^2 \mathbf{I}_{t-1} & \mathbf{W}_{t-1}^H \Sigma_{\mathbf{h}} \mathbf{w}_t \\ \mathbf{w}_t^H \Sigma_{\mathbf{h}} \mathbf{W}_{t-1} & \mathbf{w}_t^H \Sigma_{\mathbf{h}} \mathbf{w}_t + \sigma^2 \end{bmatrix}$$

$$= \begin{bmatrix} \mathbf{K}_{t-1} & \mathbf{W}_{t-1}^H \Sigma_{\mathbf{h}} \mathbf{w}_t \\ \mathbf{w}_t^H \Sigma_{\mathbf{h}} \mathbf{W}_{t-1} & \mathbf{w}_t^H \Sigma_{\mathbf{h}} \mathbf{w}_t + \sigma^2 \end{bmatrix}. \quad (49)$$

We can harness the block-matrix inversion in (50) to derive the inverse of  $\mathbf{K}_t$  [50]. By mapping the matrices  $\mathbf{A}$ ,  $\mathbf{B}$ ,  $\mathbf{C}$ , and  $\mathbf{D}$  in (49) to (50), the value of  $\mathbf{D} - \mathbf{C}\mathbf{A}^{-1}\mathbf{B}$  is expressed as

$$\mathbf{D} - \mathbf{C}\mathbf{A}^{-1}\mathbf{B}$$

$$= \mathbf{w}_t^H \Sigma_{\mathbf{h}} \mathbf{w}_t + \sigma^2 - \mathbf{w}_t^H \Sigma_{\mathbf{h}} \mathbf{W}_{t-1} \mathbf{K}_{t-1}^{-1} \mathbf{W}_{t-1}^H \Sigma_{\mathbf{h}} \mathbf{w}_t$$

$$\stackrel{(a)}{=} \mathbf{w}_t^H \Sigma_{t-1} \mathbf{w}_t + \sigma^2, \quad (51)$$

where (a) comes from the definition of  $\Sigma_{t-1}$ , i.e.,  $\Sigma_{t-1} = \Sigma_{\mathbf{h}} - \Sigma_{\mathbf{h}} \mathbf{W}_{t-1} \mathbf{K}_{t-1}^{-1} \mathbf{W}_{t-1}^H \Sigma_{\mathbf{h}}$ . Then, by substituting (50) and (51) into (49), the inverse of  $\mathbf{K}_t$  can be written as (52). Taking  $\mathbf{K}_t^{-1}$  back to the posterior kernel  $\Sigma_t$  in (10) results in

$$\Sigma_t = \Sigma_{\mathbf{h}} - \Sigma_{\mathbf{h}} \mathbf{W}_t \mathbf{K}_t^{-1} \mathbf{W}_t^H \Sigma_{\mathbf{h}}$$

$$= \Sigma_{\mathbf{h}} - \Sigma_{\mathbf{h}} \mathbf{W}_{t-1} \mathbf{K}_{t-1}^{-1} \mathbf{W}_{t-1}^H \Sigma_{\mathbf{h}} +$$

---


$$\begin{pmatrix} \mathbf{I}_t + \frac{1}{\sigma^2} \mathbf{W}_t^H \Sigma_{\mathbf{h}} \mathbf{W}_t & \frac{1}{\sigma^2} \mathbf{W}_t^H \Sigma_{\mathbf{h}} \mathbf{w}_{t+1} \\ \mathbf{0} & 1 + \frac{1}{\sigma^2} \mathbf{w}_{t+1}^H \Sigma_t \mathbf{w}_{t+1} \end{pmatrix} =$$

$$\begin{pmatrix} \mathbf{I}_t & \mathbf{0} \\ -\frac{1}{\sigma^2} \mathbf{w}_{t+1}^H \Sigma_{\mathbf{h}} \mathbf{W}_t (\mathbf{I}_t + \frac{1}{\sigma^2} \mathbf{W}_t^H \Sigma_{\mathbf{h}} \mathbf{W}_t)^{-1} & 1 \end{pmatrix} \begin{pmatrix} \mathbf{I}_t + \frac{1}{\sigma^2} \mathbf{W}_t^H \Sigma_{\mathbf{h}} \mathbf{W}_t & \frac{1}{\sigma^2} \mathbf{W}_t^H \Sigma_{\mathbf{h}} \mathbf{w}_{t+1} \\ \frac{1}{\sigma^2} \mathbf{w}_{t+1}^H \Sigma_{\mathbf{h}} \mathbf{W}_t & 1 + \frac{1}{\sigma^2} \mathbf{w}_{t+1}^H \Sigma_{\mathbf{h}} \mathbf{w}_{t+1} \end{pmatrix} \quad (48)$$


---

$$\begin{bmatrix} \mathbf{A} & \mathbf{B} \\ \mathbf{C} & \mathbf{D} \end{bmatrix}^{-1} = \begin{bmatrix} \mathbf{A}^{-1} + \mathbf{A}^{-1} \mathbf{B} (\mathbf{D} - \mathbf{C}\mathbf{A}^{-1}\mathbf{B})^{-1} \mathbf{C}\mathbf{A}^{-1} & -\mathbf{A}^{-1} \mathbf{B} (\mathbf{D} - \mathbf{C}\mathbf{A}^{-1}\mathbf{B})^{-1} \\ -(\mathbf{D} - \mathbf{C}\mathbf{A}^{-1}\mathbf{B})^{-1} \mathbf{C}\mathbf{A}^{-1} & (\mathbf{D} - \mathbf{C}\mathbf{A}^{-1}\mathbf{B})^{-1} \end{bmatrix} \quad (50)$$


---

$$\mathbf{K}_t^{-1} = \begin{bmatrix} \mathbf{K}_{t-1}^{-1} + \frac{\mathbf{K}_{t-1}^{-1} \mathbf{W}_{t-1}^H \Sigma_{\mathbf{h}} \mathbf{w}_t \mathbf{w}_t^H \Sigma_{\mathbf{h}} \mathbf{W}_{t-1} \mathbf{K}_{t-1}^{-1}}{\mathbf{w}_t^H \Sigma_{t-1} \mathbf{w}_t + \sigma^2} & -\frac{\mathbf{K}_{t-1}^{-1} \mathbf{W}_{t-1}^H \Sigma_{\mathbf{h}} \mathbf{w}_t}{\mathbf{w}_t^H \Sigma_{t-1} \mathbf{w}_t + \sigma^2} \\ -\frac{\mathbf{w}_t^H \Sigma_{\mathbf{h}} \mathbf{W}_{t-1} \mathbf{K}_{t-1}^{-1}}{\mathbf{w}_t^H \Sigma_{t-1} \mathbf{w}_t + \sigma^2} & \frac{1}{\mathbf{w}_t^H \Sigma_{t-1} \mathbf{w}_t + \sigma^2} \end{bmatrix} \quad (52)$$

$$\frac{1}{\mathbf{w}_t^H \Sigma_{t-1} \mathbf{w}_t + \sigma^2} (\mathbf{E} + \mathbf{F} + \mathbf{G} + \mathbf{H})$$

$$= \Sigma_{t-1} + \frac{1}{\mathbf{w}_t^H \Sigma_{t-1} \mathbf{w}_t + \sigma^2} (\mathbf{E} + \mathbf{F} + \mathbf{G} + \mathbf{H}), \quad (53)$$

where

$$\mathbf{E} = -\Sigma_{\mathbf{h}} \mathbf{W}_{t-1} \mathbf{K}_{t-1}^{-1} \mathbf{W}_{t-1}^H \Sigma_{\mathbf{h}} \mathbf{w}_t \mathbf{w}_t^H \Sigma_{\mathbf{h}} \mathbf{W}_{t-1} \mathbf{K}_{t-1}^{-1} \mathbf{W}_{t-1}^H \Sigma_{\mathbf{h}}$$

$$= -(\Sigma_{\mathbf{h}} - \Sigma_{t-1}) \mathbf{w}_t \mathbf{w}_t^H (\Sigma_{\mathbf{h}} - \Sigma_{t-1}),$$

$$\mathbf{F} = \Sigma_{\mathbf{h}} \mathbf{W}_{t-1} \mathbf{K}_{t-1}^{-1} \mathbf{W}_{t-1}^H \Sigma_{\mathbf{h}} \mathbf{w}_t \mathbf{w}_t^H \Sigma_{\mathbf{h}}$$

$$= (\Sigma_{\mathbf{h}} - \Sigma_{t-1}) \mathbf{w}_t \mathbf{w}_t^H \Sigma_{\mathbf{h}},$$

$$\mathbf{G} = \Sigma_{\mathbf{h}} \mathbf{w}_t \mathbf{w}_t^H \Sigma_{\mathbf{h}} \mathbf{W}_{t-1} \mathbf{K}_{t-1}^{-1} \mathbf{W}_{t-1}^H \Sigma_{\mathbf{h}}$$

$$= \Sigma_{\mathbf{h}} \mathbf{w}_t \mathbf{w}_t^H (\Sigma_{\mathbf{h}} - \Sigma_{t-1}),$$

$$\mathbf{H} = -\Sigma_{\mathbf{h}} \mathbf{w}_t \mathbf{w}_t^H \Sigma_{\mathbf{h}}.$$

It is straightforward to verify that the sum of  $\mathbf{E}$ ,  $\mathbf{F}$ ,  $\mathbf{G}$ , and  $\mathbf{H}$  is exactly  $-\Sigma_{t-1} \mathbf{w}_t \mathbf{w}_t^H \Sigma_{t-1}$ . By substituting  $\mathbf{E}$ ,  $\mathbf{F}$ ,  $\mathbf{G}$ , and  $\mathbf{H}$  into (53), we have

$$\Sigma_t = \Sigma_{t-1} - \frac{\Sigma_{t-1} \mathbf{w}_t \mathbf{w}_t^H \Sigma_{t-1}}{\mathbf{w}_t^H \Sigma_{t-1} \mathbf{w}_t + \sigma^2}, \quad (54)$$

which completes the proof.

#### APPENDIX C PROOF OF THEOREM 2

**Theorem 2** can be proved by the contradiction method. Suppose there exists an index  $k$  such that  $n_k \geq p_k + 1$ . Due to the constraint that  $\sum_{k=1}^K n_k = \sum_{k=1}^K p_k = Q$ , there must exist  $k'$  such that  $k' \neq k$  and  $n_{k'} < p_{k'}$ , otherwise  $\sum_{k=1}^K n_k$  will be larger than  $\sum_{k=1}^K p_k$ . Note that  $p_{k'}$  is non-zero since  $p_{k'} > n_{k'} \geq 0$ . In this context, the water level can be expressed as  $\beta = p_{k'} + \frac{\sigma^2}{\lambda_{k'}}$  and the  $k'$ -th ice level  $\frac{\sigma^2}{\lambda_{k'}}$  should be smaller than  $\beta$  because

$$\frac{\sigma^2}{\lambda_{k'}} = n_{k'} + \frac{\sigma^2}{\lambda_{k'}} < p_{k'} + \frac{\sigma^2}{\lambda_{k'}} = \beta. \quad (55)$$

Then, consider the  $k$ -th ice level  $\frac{\sigma^2}{\lambda_k^Q}$ . Since  $n_k \geq p_k + 1$ , we have the following inequality:

$$\begin{aligned} \frac{\sigma^2}{\lambda_k^Q} &= n_k + \frac{\sigma^2}{\lambda_k} \geq p_k + \frac{\sigma^2}{\lambda_k} + 1 = \left( \beta - \frac{\sigma^2}{\lambda_k} \right)^+ + \frac{\sigma^2}{\lambda_k} + 1 \\ &\stackrel{(a)}{\geq} \beta + 1, \end{aligned} \quad (56)$$

where the inequality (a) holds because  $\left( \beta - \frac{\sigma^2}{\lambda_k} \right)^+ \geq \beta - \frac{\sigma^2}{\lambda_k}$ . Combining equations (55) and (56), we arrive at

$$\frac{\sigma^2}{\lambda_k^Q} > \frac{\sigma^2}{\lambda_{k'}^Q} + 1. \quad (57)$$

We introduce the following **Lemma 9** to evaluate the inequality (57).

**Lemma 9:** For the  $k$ -th eigenvalue  $\lambda_k^t$  obtained at the  $t$ -th timeslot, if  $n_k^t > 0$ , we have the inequality

$$\frac{\sigma^2}{\lambda_{k'}^t} + 1 \geq \frac{\sigma^2}{\lambda_k^t}, \quad (58)$$

hold for all  $k' \in \{1, 2, \dots, K\}$ .

*Proof:* Since  $n_k^t > 0$ , the  $k$ -th eigenvector is selected by the ice-filling algorithm at least once. Let  $t' < t$  denote the latest timeslot before  $t$  when the  $k$ -th eigenvector is selected for pilot transmission such that  $n_k^{t'} = n_k^t - 1$  and  $n_k^{t'+1} = n_k^t$ .

Suppose there exists  $k'$  such that  $\frac{\sigma^2}{\lambda_{k'}^t} < \frac{\sigma^2}{\lambda_k^t} - 1$ , then we have

$$\frac{\sigma^2}{\lambda_{k'}^{t'}} \stackrel{(b)}{\leq} \frac{\sigma^2}{\lambda_{k'}^t} \stackrel{(c)}{<} \frac{\sigma^2}{\lambda_k} + n_k^t - 1 = \frac{\sigma^2}{\lambda_k} + n_k^{t'} = \frac{\sigma^2}{\lambda_{k'}^{t'}}, \quad (59)$$

where (b) holds because the ice-level  $\frac{\sigma^2}{\lambda_{k'}^t}$  is non-decreasing w.r.t the timeslot  $t$ , and (c) holds given that  $\frac{\sigma^2}{\lambda_k} + n_k^t = \frac{\sigma^2}{\lambda_{k'}^t}$ . The inequality  $\frac{\sigma^2}{\lambda_{k'}^t} < \frac{\sigma^2}{\lambda_{k'}^{t'}}$  in (59) contradicts the eigenvector selection principle of the ice-filling algorithm that  $\lambda_{k'}^{t'}$  should be the largest over the eigenvalue set  $\{\lambda_1^{t'}, \lambda_2^{t'}, \dots, \lambda_K^{t'}\}$ . Therefore,  $\frac{\sigma^2}{\lambda_{k'}^t}$  should be no less than  $\frac{\sigma^2}{\lambda_k^t} - 1$  for all  $k'$ , which completes the proof. ■

Comparing (57) and (58), it is clear that (57) contradicts **Lemma 9** given that  $n_k \geq p_k + 1 > 0$ . Therefore,  $n_k$  should be smaller than  $p_k + 1$ .

We adopt the same method to prove that  $n_k > p_k - 1$ . Specifically, suppose there is  $k$  such that  $n_k \leq p_k - 1$ . Then there must exist  $k' \neq k$  such that  $n_{k'} > p_{k'}$ . From the inequality  $n_k \leq p_k - 1$ , we know that the ice level  $\frac{\sigma^2}{\lambda_k^Q}$  satisfies the inequality

$$\frac{\sigma^2}{\lambda_k^Q} = n_k + \frac{\sigma^2}{\lambda_k} \leq p_k + \frac{\sigma^2}{\lambda_k} - 1 \stackrel{(b)}{=} \beta - 1, \quad (60)$$

where (b) arises because  $p_k$  is greater than 0. On the other hand, from the inequality  $n_{k'} > p_{k'}$ , we get

$$\frac{\sigma^2}{\lambda_{k'}^Q} = n_{k'} + \frac{\sigma^2}{\lambda_{k'}} > p_{k'} + \frac{\sigma^2}{\lambda_{k'}} \geq \beta. \quad (61)$$

Combining (60) and (61), we get

$$\frac{\sigma^2}{\lambda_{k'}^Q} \geq \frac{\sigma^2}{\lambda_k^Q} + 1, \quad (62)$$

which contradicts **Lemma 9** because  $n_{k'} > p_{k'} \geq 0$ . As a result,  $n_k$  should be larger than  $p_k - 1$ , and thereby we get

$$|n_k - p_k| < 1, \quad (63)$$

which completes the proof.

#### APPENDIX D PROOF OF LEMMA 3

Substituting  $\mathbf{W} = \mathbf{U}_K \mathbf{P}$  and  $\Sigma_{\mathbf{h}} = \mathbf{U}_K \Lambda_K \mathbf{U}_K^H$  into the definition of  $\Sigma_{\mathbf{h}|\mathbf{y}}$ , we get

$$\begin{aligned} \Sigma_{\mathbf{h}|\mathbf{y}} &= \Sigma_{\mathbf{h}} - \Sigma_{\mathbf{h}} \mathbf{W} (\mathbf{W}^H \Sigma_{\mathbf{h}} \mathbf{W} + \sigma^2 \mathbf{I}_Q)^{-1} \mathbf{W}^H \Sigma_{\mathbf{h}} \\ &= \mathbf{U}_K \Lambda_K \mathbf{U}_K^H - \mathbf{U}_K \Lambda_K \mathbf{U}_K^H \mathbf{U}_K \mathbf{P} (\mathbf{P}^H \mathbf{U}_K^H \mathbf{U}_K \Lambda_K \mathbf{U}_K^H \mathbf{U}_K \mathbf{P} \\ &\quad + \sigma^2 \mathbf{I}_Q)^{-1} \mathbf{P}^H \mathbf{U}_K^H \mathbf{U}_K \Lambda_K \mathbf{U}_K^H \\ &= \mathbf{U}_K \underbrace{\left( \Lambda_K - \Lambda_K \mathbf{P} (\mathbf{P}^H \Lambda_K \mathbf{P} + \sigma^2 \mathbf{I}_Q)^{-1} \mathbf{P}^H \Lambda_K \right)}_{\Lambda_{\mathbf{h}|\mathbf{y}}} \mathbf{U}_K^H. \end{aligned} \quad (64)$$

Note that matrices  $\Lambda_K$  and  $\mathbf{P}$  are both diagonal. Hence, it can be directly proved that

$$\Lambda_{\mathbf{h}|\mathbf{y}} = \text{diag} \left( \frac{\lambda_1 \sigma^2}{p_1 \lambda_1 + \sigma^2}, \dots, \frac{\lambda_K \sigma^2}{p_K \lambda_K + \sigma^2} \right). \quad (65)$$

Therefore, given that  $\mathbf{U}_K^H \mathbf{U}_K = \mathbf{I}_K$ , the MSE achieved by water-filling can be derived as

$$\text{Tr}(\Sigma_{\mathbf{h}|\mathbf{y}}) = \text{Tr}(\Lambda_{\mathbf{h}|\mathbf{y}}) = \sum_{k=1}^K \frac{\lambda_k \sigma^2}{p_k \lambda_k + \sigma^2}. \quad (66)$$

Particularly, as  $Q \rightarrow +\infty$ , the water-filling principle asymptotically allocates equal power  $Q/K$  to all eigenvectors [45], rendering the estimation error decays at a rate of  $\mathcal{O}\left(\sum_{k=1}^K \frac{K \sigma^2}{Q}\right) = \mathcal{O}(K^2 Q^{-1})$ . This completes the proof.

#### APPENDIX E PROOF OF LEMMA 4

We first express the observation matrix designed by the ice-filling algorithm as  $\mathbf{W} = \mathbf{U}_K \mathbf{S}$ . Here,  $\mathbf{S} \in \{0, 1\}^{K \times Q}$  represents a switch matrix, each column of which contains one non-zero entry, i.e.,  $\mathbf{S}(k, q) \in \{0, 1\}$  and  $\sum_{k=1}^K \mathbf{S}(k, q) = 1$ . In particular,  $\mathbf{S}(k, q) = 1$  implies that the  $k$ -th eigenvector,  $\mathbf{u}_k$ , is assigned to the  $q$ -th observation vector. Based on this definition, we can prove that

$$\mathbf{S} \mathbf{S}^H = \mathbf{N} = \text{diag}(n_1, n_2, \dots, n_K), \quad (67)$$

given that  $n_k$  ( $k \in \{1, 2, \dots, K\}$ ) stands for the number of times that the eigenvector  $\mathbf{u}_k$  is assigned to  $\mathbf{W}$  by **Algorithm 2**. Then, by substituting  $\mathbf{W} = \mathbf{U}_K \mathbf{S}$  and  $\Sigma_{\mathbf{h}} = \mathbf{U}_K \Lambda_K \mathbf{U}_K^H$  into (10), we can express  $\Sigma_{\mathbf{h}|\mathbf{y}}$  as

$$\Sigma_{\mathbf{h}|\mathbf{y}} = \mathbf{U}_K \Lambda_{\mathbf{h}|\mathbf{y}} \mathbf{U}_K^H, \quad (68)$$

where  $\Lambda_{\mathbf{h}|\mathbf{y}} = \Lambda_K - \Lambda_K \mathbf{S} (\mathbf{S}^H \Lambda_K \mathbf{S} + \sigma^2 \mathbf{I}_Q)^{-1} \mathbf{S}^H \Lambda_K$ . Moreover, the Sherman-Morrison-Woodbury formula [50]

$$(\mathbf{A} + \mathbf{XRY})^{-1} = \mathbf{A}^{-1} - \mathbf{A}^{-1} \mathbf{X} (\mathbf{R}^{-1} + \mathbf{Y} \mathbf{A}^{-1} \mathbf{X})^{-1} \mathbf{Y} \mathbf{A}^{-1} \quad (69)$$

allows us to rewrite  $\Lambda_{\mathbf{h}|\mathbf{y}}$  as

$$\begin{aligned} \Lambda_{\mathbf{h}|\mathbf{y}} &= \Lambda_K - \frac{1}{\sigma^2} \Lambda_K \mathbf{S} \mathbf{S}^H \Lambda_K \\ &\quad + \frac{1}{\sigma^4} \Lambda_K \mathbf{S} \mathbf{S}^H \left( \Lambda_K^{-1} + \frac{1}{\sigma^2} \mathbf{S} \mathbf{S}^H \right)^{-1} \mathbf{S} \mathbf{S}^H \Lambda_K \\ &\stackrel{(a)}{=} \Lambda_K - \frac{1}{\sigma^2} \Lambda_K \mathbf{N} \Lambda_K + \frac{1}{\sigma^4} \Lambda_K \mathbf{N} \left( \Lambda_K^{-1} + \frac{1}{\sigma^2} \mathbf{N} \right)^{-1} \mathbf{N} \Lambda_K, \\ &\stackrel{(b)}{=} \text{diag} \left( \frac{\lambda_1 \sigma^2}{n_1 \lambda_1 + \sigma^2}, \dots, \frac{\lambda_K \sigma^2}{n_K \lambda_K + \sigma^2} \right), \end{aligned} \quad (70)$$

where (a) holds since  $\mathbf{S} \mathbf{S}^H = \mathbf{N}$ , and the equation (b) comes directly from the fact the matrices  $\Lambda_K$  and  $\mathbf{N}$  are both diagonal. In conclusion, the MSE achieved by the ice-filling algorithm is  $\text{Tr}(\Lambda_{\mathbf{h}|\mathbf{y}}) = \sum_{k=1}^K \frac{\lambda_k \sigma^2}{n_k \lambda_k + \sigma^2}$ . Moreover, since  $|n_k - p_k| < 1$ , the asymptotic estimation error is naturally  $\mathcal{O}(K^2 Q^{-1})$  as  $Q \rightarrow +\infty$ , which completes the proof.

#### APPENDIX F PROOF OF THEOREM 3

We use the **Theorem 2** to upper-bound the asymptotic MSE difference as  $Q \rightarrow +\infty$ , i.e.,

$$\begin{aligned} |\delta_{\text{wf}} - \delta_{\text{if}}| &= \left| \sum_{k=1}^K \frac{\lambda_k \sigma^2}{p_k \lambda_k + \sigma^2} - \sum_{k=1}^K \frac{\lambda_k \sigma^2}{n_k \lambda_k + \sigma^2} \right| \\ &\leq \sum_{k=1}^K \left| \frac{\lambda_k \sigma^2}{p_k \lambda_k + \sigma^2} - \frac{\lambda_k \sigma^2}{n_k \lambda_k + \sigma^2} \right| \\ &= \sum_{k=1}^K \left| \frac{\lambda_k^2 \sigma^2 (p_k - n_k)}{(p_k \lambda_k + \sigma^2)(n_k \lambda_k + \sigma^2)} \right| \\ &\stackrel{(a)}{<} \sum_{k=1}^K \left| \frac{\lambda_k^2 \sigma^2}{(p_k \lambda_k + \sigma^2)((p_k - 1) \lambda_k + \sigma^2)} \right|, \end{aligned} \quad (71)$$

where (a) holds due to the facts that  $|n_k - p_k| < 1$  and  $n_k > p_k - 1 > 0$  when  $Q \rightarrow +\infty$ . Moreover, the water-filling principle tends to allocate equal power to all channels, i.e.,  $p_k \rightarrow Q/K$  for large  $Q$  [45]. Thereafter, the asymptotic upper-bound of the MSE difference becomes

$$|\delta_{\text{wf}} - \delta_{\text{if}}| < \sum_{k=1}^K \frac{K^2 \sigma^2}{Q^2} = \mathcal{O}(K^3 Q^{-2}). \quad (72)$$

#### APPENDIX G PROOF OF LEMMA 5

Let  $\Sigma_{\mathbf{h}} = \mathbf{U}_K \Lambda_K \mathbf{U}_K^H$  denote the eigenvalue decomposition of the rank- $K$  kernel  $\Sigma_{\mathbf{h}}$ , wherein  $\mathbf{U}_K \in \mathbb{C}^{M \times K}$  and  $\Lambda_K \in \mathbb{C}^{M \times M}$ . According to the extension of the Sherman-Morrison-Woodbury formula in (69), the MSE achieved by the proposed algorithms can be rewritten as

$$\mathbb{E}(\|\mu_{\mathbf{h}|\mathbf{y}} - \mathbf{h}\|_2^2) = \text{Tr}(\Sigma_{\mathbf{h}|\mathbf{y}})$$

$$= \text{Tr} \left( \mathbf{U}_K \left( \Lambda_K^{-1} + \frac{1}{\sigma^2} \mathbf{U}_K^H \mathbf{W} \mathbf{W}^H \mathbf{U}_K \right)^{-1} \mathbf{U}_K^H \right). \quad (73)$$

For the randomly generated observation matrix  $\mathbf{W}$  in both the amplitude-and-phase controllable and phase-only controllable cases, following the asymptotic orthogonality principle, we have  $\mathbf{W} \mathbf{W}^H \approx \frac{Q}{M} \mathbf{I}_M$  when  $Q$  is sufficiently large. In this case, the posterior kernel can be approximated by

$$\begin{aligned} \Sigma_{\mathbf{h}|\mathbf{y}} &\approx \mathbf{U}_K \left( \Lambda_K^{-1} + \frac{1}{\sigma^2} \frac{Q}{M} \mathbf{U}_K^H \mathbf{U}_K \right)^{-1} \mathbf{U}_K^H = \\ &\mathbf{U}_K \text{diag} \left( \frac{1}{\frac{1}{\lambda_1} + \frac{Q}{M\sigma^2}}, \frac{1}{\frac{1}{\lambda_2} + \frac{Q}{M\sigma^2}}, \dots, \frac{1}{\frac{1}{\lambda_K} + \frac{Q}{M\sigma^2}} \right) \mathbf{U}_K^H. \end{aligned} \quad (74)$$

Therefore, by substituting (74) into (73), the MSE  $\delta_{\text{rnd}}$  is given by

$$\delta_{\text{rnd}} \approx \sum_{k=1}^K \frac{1}{\frac{1}{\lambda_k} + \frac{Q}{M\sigma^2}} = \sum_{k=1}^K \frac{\lambda_k \sigma^2}{\frac{Q}{M} \lambda_k + \sigma^2}, \quad (75)$$

which completes the proof.

#### APPENDIX H PROOF OF LEMMA 6

Given a prior kernel  $\Sigma$  as the input of the proposed estimator, the squared error of channel estimation can be derived as

$$\begin{aligned} \|\mu_{\mathbf{h}|\mathbf{y}} - \mathbf{h}\|_2^2 &= \left\| \Sigma \mathbf{W} (\mathbf{W}^H \Sigma \mathbf{W} + \sigma^2 \mathbf{I}_Q)^{-1} \mathbf{y} - \mathbf{h} \right\|_2^2 \\ &\stackrel{(a)}{=} \left\| \left( \Sigma \mathbf{W} (\mathbf{W}^H \Sigma \mathbf{W} + \sigma^2 \mathbf{I}_Q)^{-1} \mathbf{W}^H - \mathbf{I}_M \right) \mathbf{h} \right. \\ &\quad \left. + \Sigma \mathbf{W} (\mathbf{W}^H \Sigma \mathbf{W} + \sigma^2 \mathbf{I}_Q)^{-1} \mathbf{z} \right\|_2^2 \\ &\stackrel{(b)}{=} \left\| (\mathbf{\Pi}^H \mathbf{W}^H - \mathbf{I}_M) \mathbf{h} + \mathbf{\Pi}^H \mathbf{z} \right\|_2^2, \end{aligned} \quad (76)$$

where (a) holds since  $\mathbf{y} = \mathbf{W}^H \mathbf{h} + \mathbf{z}$  and (b) holds by defining  $\mathbf{\Pi} = (\mathbf{W}^H \Sigma \mathbf{W} + \sigma^2 \mathbf{I}_Q)^{-1} \mathbf{W}^H \Sigma$ , which can be viewed as a matrix function with respect to the artificial kernel  $\Sigma$ . Next, recalling properties  $\mathbf{z} \sim \mathcal{CN}(\mathbf{0}_Q, \sigma^2 \mathbf{I}_Q)$  and  $\mathbb{E}(\mathbf{h} \mathbf{h}^H) = \Sigma_{\mathbf{h}}$ , the MSE  $\hat{\delta}$  under imperfect kernel can be derived as

$$\hat{\delta} = \text{Tr} \left( (\mathbf{\Pi}^H \mathbf{W}^H - \mathbf{I}_M) \Sigma_{\mathbf{h}} (\mathbf{W} \mathbf{\Pi} - \mathbf{I}_M) \right) + \sigma^2 \text{Tr}(\mathbf{\Pi}^H \mathbf{\Pi}), \quad (77)$$

where the equality holds since  $\|\mathbf{x}\|_2^2 = \text{Tr}(\mathbf{x} \mathbf{x}^H)$  for any vector  $\mathbf{x}$ , which completes the proof.

#### APPENDIX I PROOF OF COROLLARY 1

Observing (36), one can find that the MSE  $\hat{\delta}$  is a quadratic form w.r.t matrix  $\mathbf{\Pi}$ . Thus, the lower-bound of the MSE can be achieved by finding a  $\Sigma$  such that  $\frac{\partial \hat{\delta}}{\partial \mathbf{\Pi}} = \mathbf{0}_{Q \times M}$  holds. According to (36), the partial derivative of  $\hat{\delta}$  w.r.t  $\mathbf{\Pi}$  can be derived as

$$\frac{\partial \hat{\delta}}{\partial \mathbf{\Pi}} = (\mathbf{W}^H \Sigma_{\mathbf{h}} \mathbf{W} + \sigma^2 \mathbf{I}_Q)^* \mathbf{\Pi}^* - (\mathbf{W}^H \Sigma_{\mathbf{h}})^*. \quad (78)$$



By letting  $\frac{\partial \hat{\delta}}{\partial \Pi} = \mathbf{0}_{PM \times N}$  and substituting  $\Pi = (\mathbf{W}^H \Sigma \mathbf{W} + \sigma^2 \mathbf{I}_Q)^{-1} \mathbf{W}^H \Sigma$  into (78), the original proof can be reduced to prove that

$$(\mathbf{W}^H \Sigma_h \mathbf{W} + \sigma^2 \mathbf{I}_Q)^{-1} \mathbf{W}^H \Sigma_h = (\mathbf{W}^H \Sigma \mathbf{W} + \sigma^2 \mathbf{I}_Q)^{-1} \mathbf{W}^H \Sigma. \quad (79)$$

Since the proposed method does not depend on the value of noise power, (79) should hold for arbitrary  $\sigma^2$ . By considering the special case when  $\sigma^2 \rightarrow \infty$ , (79) is equivalent to

$$\mathbf{W}^H (\Sigma_h - \Sigma) = \mathbf{0}_{Q \times M} \quad (80)$$

Furthermore, since our derivation also does not impose the specific form of  $\mathbf{W}$ ,  $\Sigma = \Sigma_h$  is necessary to make the equation always hold. By substituting  $\Sigma = \Sigma_h$  into (36), the lower-bound of the achievable MSE is exactly the trace of the posterior kernel  $\Sigma_{\text{hly}}$ , rewritten as

$$\min_{\mu, \Sigma} \hat{\delta} = \text{Tr}(\Sigma_h) - \text{Tr}\left(\Sigma_h \mathbf{W} (\mathbf{W}^H \Sigma_h \mathbf{W} + \sigma^2 \mathbf{I}_Q)^{-1} \mathbf{W}^H \Sigma_h\right), \quad (81)$$

which completes the proof.

#### APPENDIX J PROOF OF LEMMA 7

Comparing (37) and (36), we only need to prove that  $\mathbf{W}\Pi = \Omega \hat{\Sigma}_h$  and  $\Pi^H \Pi = \hat{\Sigma}_h \Xi \hat{\Sigma}_h$  in the case when  $\Sigma = \hat{\Sigma}_h$ . Due to the positive semi-definition of  $\Sigma_h$ , the inversion of  $\hat{\Sigma}_h = \Sigma_h + \sigma_h^2 \mathbf{I}_M$  exists. Thus, by applying the Sherman-Morrison-Woodbury formula in (69) for the term  $(\mathbf{W}^H \hat{\Sigma}_h \mathbf{W} + \sigma^2 \mathbf{I}_Q)^{-1}$ ,  $\mathbf{W}\Pi$  can be reorganized as

$$\begin{aligned} \mathbf{W}\Pi &= \mathbf{W} (\mathbf{W}^H \hat{\Sigma}_h \mathbf{W} + \sigma^2 \mathbf{I}_Q)^{-1} \mathbf{W}^H \hat{\Sigma}_h \\ &= \mathbf{W} \left( \frac{1}{\sigma^2} \mathbf{I}_Q - \frac{1}{\sigma^4} \mathbf{W}^H \left( \hat{\Sigma}_h^{-1} + \frac{1}{\sigma^2} \mathbf{W} \mathbf{W}^H \right)^{-1} \mathbf{W} \right) \mathbf{W}^H \hat{\Sigma}_h \\ &= \left( \frac{\mathbf{W} \mathbf{W}^H}{\sigma^2} - \frac{\mathbf{W} \mathbf{W}^H}{\sigma^4} \left( \hat{\Sigma}_h^{-1} + \frac{\mathbf{W} \mathbf{W}^H}{\sigma^2} \right)^{-1} \mathbf{W} \mathbf{W}^H \right) \hat{\Sigma}_h, \end{aligned} \quad (82)$$

which is equal to  $\Omega \hat{\Sigma}_h$  and obviously the is a function of  $\mathbf{W} \mathbf{W}^H$ . Using the same matrix techniques as (82), we can prove that

$$\begin{aligned} \Pi^H \Pi &= \hat{\Sigma}_h \mathbf{W} (\mathbf{W}^H \hat{\Sigma}_h \mathbf{W} + \sigma^2 \mathbf{I}_Q)^{-2} \mathbf{W}^H \hat{\Sigma}_h \\ &= \hat{\Sigma}_h \mathbf{W} \left( \frac{1}{\sigma^2} \mathbf{I}_Q - \frac{1}{\sigma^4} \mathbf{W}^H \left( \hat{\Sigma}_h^{-1} + \frac{\mathbf{W} \mathbf{W}^H}{\sigma^2} \right)^{-1} \mathbf{W} \right)^2 \mathbf{W}^H \hat{\Sigma}_h \\ &= \hat{\Sigma}_h \left( \frac{\mathbf{W} \mathbf{W}^H}{\sigma^4} - 2 \frac{\mathbf{W} \mathbf{W}^H}{\sigma^6} \left( \hat{\Sigma}_h^{-1} + \frac{\mathbf{W} \mathbf{W}^H}{\sigma^2} \right)^{-1} \mathbf{W} \mathbf{W}^H + \frac{\mathbf{W} \mathbf{W}^H}{\sigma^8} \left( \left( \hat{\Sigma}_h^{-1} + \frac{\mathbf{W} \mathbf{W}^H}{\sigma^2} \right)^{-1} \mathbf{W} \mathbf{W}^H \right)^2 \right) \hat{\Sigma}_h, \end{aligned} \quad (83)$$

which is equal to  $\hat{\Sigma}_h \Xi \hat{\Sigma}_h$  and obviously is a function of  $\mathbf{W} \mathbf{W}^H$ . This completes the proof.

#### APPENDIX K PROOF OF LEMMA 8

Let  $\Sigma_h = \mathbf{U} \Lambda \mathbf{U}^H$  denote the complete eigenvalue decomposition of the kernel  $\Sigma_h$ , wherein  $\mathbf{U} \in \mathbb{C}^{M \times M}$  and  $\Lambda = \text{diag}\{\lambda_1, \dots, \lambda_M\}$  with  $\lambda_m = 0$  for  $K < m \leq M$ . According to the analyses in Appendices D, E, and G, the term  $\mathbf{W} \mathbf{W}^H$  for the water-filling estimator, ice-filling estimator, and random estimator can be respectively written as

$$\mathbf{W}_{\text{wf}} \mathbf{W}_{\text{wf}}^H = \mathbf{U} \hat{\mathbf{P}} \hat{\mathbf{P}}^H \mathbf{U}^H, \quad (84a)$$

$$\mathbf{W}_{\text{if}} \mathbf{W}_{\text{if}}^H = \mathbf{U} \hat{\mathbf{N}} \mathbf{U}^H, \quad (84b)$$

$$\mathbf{W}_{\text{rnd}} \mathbf{W}_{\text{rnd}}^H \approx \frac{Q}{M} \mathbf{I}_M = \mathbf{U} \left( \frac{Q}{M} \mathbf{I}_M \right) \mathbf{U}^H. \quad (84c)$$

where  $\hat{\mathbf{P}} = \text{diag}(\sqrt{\hat{p}_1}, \dots, \sqrt{\hat{p}_M})$  is the power allocated to the  $M$  eigenvectors of  $\hat{\Sigma}_h$  and  $\hat{\mathbf{N}} = \text{diag}(\hat{n}_1, \dots, \hat{n}_M)$  is the pilot-reuse-frequency matrix, as defined in (67). It is clear from (84) that the terms  $\mathbf{W} \mathbf{W}^H$  in the three cases share a general form  $\mathbf{W} \mathbf{W}^H = \mathbf{U} \Psi \mathbf{U}^H$  wherein  $\Psi = \text{diag}(\psi_1, \dots, \psi_M)$  is a diagonal matrix. Therefore, the proof of **Lemma 8** can be obtained by replacing  $\Psi$  with the corresponding terms  $\hat{\mathbf{P}} \hat{\mathbf{P}}^H$ ,  $\hat{\mathbf{N}}$ , and  $\frac{Q}{M} \mathbf{I}_M$ , respectively. It allows us focus on the general proof based on the common expression  $\mathbf{U} \Psi \mathbf{U}^H$ , which is given as follows.

Recalling the useful expression in **Lemma 7**, by substituting  $\mathbf{W} \mathbf{W}^H = \mathbf{U} \Psi \mathbf{U}^H$ ,  $\Sigma_h = \mathbf{U} \Lambda \mathbf{U}^H$ , and  $\hat{\Sigma}_h = \Sigma_h + \sigma_h^2 \mathbf{I}_M$  into  $\Omega$  in (38) and  $\Xi$  in (39), we arrive at

$$\begin{aligned} \Omega \hat{\Sigma}_h &= \mathbf{U} \left( \frac{\Psi}{\sigma^2} - \frac{\Psi}{\sigma^4} \left( (\Lambda + \sigma_h^2 \mathbf{I}_M)^{-1} + \frac{\Psi}{\sigma^2} \right)^{-1} \Psi \right) \Lambda \mathbf{U}^H \\ &= \mathbf{U} \text{diag} \left( \frac{\psi_1 (\lambda_1 + \sigma_h^2)}{\sigma^2 + \psi_1 (\lambda_1 + \sigma_h^2)}, \dots, \frac{\psi_M (\lambda_M + \sigma_h^2)}{\sigma^2 + \psi_M (\lambda_M + \sigma_h^2)} \right) \mathbf{U}^H \\ &= \mathbf{U} \Lambda_{\Omega} \mathbf{U}^H, \end{aligned} \quad (85)$$

$$\begin{aligned} \hat{\Sigma}_h \Xi \hat{\Sigma}_h &= \mathbf{U} (\Lambda + \sigma_h^2 \mathbf{I}_M) \times \\ &\quad \left( \frac{\Psi}{\sigma^4} - 2 \frac{\Psi}{\sigma^6} \left( (\Lambda + \sigma_h^2 \mathbf{I}_L)^{-1} + \frac{\Psi}{\sigma^2} \right)^{-1} \Psi + \frac{\Psi}{\sigma^8} \left( \left( (\Lambda + \sigma_h^2 \mathbf{I}_L)^{-1} + \frac{\Psi}{\sigma^2} \right)^{-1} \Psi \right)^2 \right) (\Lambda + \sigma_h^2 \mathbf{I}_M) \mathbf{U}^H = \\ &\quad \mathbf{U} \text{diag} \left( \frac{\psi_1 (\lambda_1 + \sigma_h^2)^2}{(\psi_1 (\lambda_1 + \sigma_h^2) + \sigma^2)^2}, \dots, \frac{\psi_M (\lambda_M + \sigma_h^2)^2}{(\psi_M (\lambda_M + \sigma_h^2) + \sigma^2)^2} \right) \mathbf{U}^H \\ &= \mathbf{U} \Lambda_{\Xi} \mathbf{U}^H, \end{aligned} \quad (86)$$

where  $\Lambda_{\Omega}$  and  $\Lambda_{\Xi}$  are both  $M$ -dimensional diagonal matrices. By substituting the above  $\Omega \hat{\Sigma}_h$ ,  $\hat{\Sigma}_h \Xi \hat{\Sigma}_h$ , and  $\Sigma_h = \mathbf{U} \Lambda \mathbf{U}^H$  into  $\hat{\delta}$  in (37), we obtain

$$\begin{aligned} \hat{\delta} &= \text{Tr}((\Lambda_{\Omega} - \mathbf{I}_M) \Lambda (\Lambda_{\Omega} - \mathbf{I}_M)) + \sigma^2 \text{Tr}(\Lambda_{\Xi}) \\ &= \sigma^2 \sum_{m=1}^M \frac{\lambda_m \sigma^2 + \psi_m (\lambda_m + \sigma_h^2)^2}{(\psi_m (\lambda_m + \sigma_h^2) + \sigma^2)^2} \\ &= \sigma^2 \sum_{k=1}^K \frac{\lambda_k \sigma^2 + \psi_k (\lambda_k + \sigma_h^2)^2}{(\psi_k (\lambda_k + \sigma_h^2) + \sigma^2)^2} + \sum_{m=K+1}^M \frac{\psi_m \sigma^2 \sigma_h^4}{(\psi_m \sigma_h^2 + \sigma^2)^2}, \end{aligned} \quad (87)$$

where the second equality holds since  $\lambda_m = 0$  for all  $m > K$ . According to (84), for the water-filling estimator, ice-filling estimator, and random estimator, we can replace the  $\psi_m$  in (87) with  $\hat{p}_m$ ,  $\hat{r}_m$ , and  $\frac{Q}{M}$  to obtain  $\hat{\delta}_{\text{wf}}$ ,  $\hat{\delta}_{\text{if}}$ , and  $\hat{\delta}_{\text{rnd}}$ , respectively. According to (87), it is obvious that  $\hat{\delta} \stackrel{Q \rightarrow +\infty}{=} \mathcal{O}(\sigma^2 M^2 Q^{-1})$  holds for the three estimators. This completes the proof.

## REFERENCES

- [1] J. Zhang, E. Björnson, M. Matthaiou, D. W. K. Ng, H. Yang, and D. J. Love, "Prospective multiple antenna technologies for beyond 5G," *IEEE J. Sel. Areas Commun.*, vol. 38, no. 8, pp. 1637–1660, Aug. 2020.
- [2] N. Shlezinger, G. C. Alexandropoulos, M. F. Imani, Y. C. Eldar, and D. R. Smith, "Dynamic metasurface antennas for 6G extreme massive MIMO communications," *IEEE Wireless Commun.*, vol. 28, no. 2, pp. 106–113, Apr. 2021.
- [3] C.-X. Wang, X. You, X. Gao, X. Zhu, Z. Li, C. Zhang, H. Wang, Y. Huang, Y. Chen, H. Haas, J. S. Thompson, E. G. Larsson, M. D. Renzo, W. Tong, P. Zhu, X. Shen, H. V. Poor, and L. Hanzo, "On the road to 6G: Visions, requirements, key technologies, and testbeds," *IEEE Commun. Surv. Tutorials*, vol. 25, no. 2, pp. 905–974, Secondquarter 2023.
- [4] C. Han, L. Yan, and J. Yuan, "Hybrid beamforming for terahertz wireless communications: Challenges, architectures, and open problems," *IEEE Wireless Commun.*, vol. 28, no. 4, pp. 198–204, Aug. 2021.
- [5] R. M. Dreifuerst and R. W. Heath, "Massive MIMO in 5G: How beamforming, codebooks, and feedback enable larger arrays," *IEEE Commun. Mag.*, vol. 61, no. 12, pp. 18–23, Dec. 2023.
- [6] K. Ying, Z. Gao, S. Chen, X. Gao, M. Matthaiou, R. Zhang, and R. Schober, "Reconfigurable massive MIMO: Harnessing the power of the electromagnetic domain for enhanced information transfer," *IEEE Wireless Commun.*, pp. 1–8, Mar. 2023.
- [7] M. Cui and L. Dai, "Channel estimation for extremely large-scale MIMO: Far-field or near-field?" *IEEE Trans. Commun.*, vol. 70, no. 4, pp. 2663–2677, Apr. 2022.
- [8] M. Cui, Z. Wu, Y. Lu, X. Wei, and L. Dai, "Near-field MIMO communications for 6G: Fundamentals, challenges, potentials, and future directions," *IEEE Commun. Mag.*, vol. 61, no. 1, pp. 40–46, Jan. 2023.
- [9] Z. Zhang and L. Dai, "Pattern-division multiplexing for multi-user continuous-aperture MIMO," *IEEE J. Sel. Areas Commun.*, vol. 41, no. 8, pp. 2350–2366, Aug. 2023.
- [10] Y. Liu, M. Zhang, T. Wang, A. Zhang, and M. Debbah, "Densifying MIMO: Channel modeling, physical constraints, and performance evaluation for holographic communications," *IEEE J. Sel. Areas Commun.*, Apr. 2023.
- [11] D. González-Ovejero, G. Minatti, G. Chattopadhyay, and S. Maci, "Multibeam by metasurface antennas," *IEEE Trans. Antennas Propag.*, vol. 65, no. 6, pp. 2923–2930, Jun. 2017.
- [12] R.-B. Hwang, "Binary meta-hologram for a reconfigurable holographic metamaterial antenna," *Sci. Rep.*, vol. 10, no. 1, p. 8586, 2020.
- [13] C. Liaskos, S. Nie, A. Tsioliaridou, A. Pitsillides, S. Ioannidis, and I. Akyildiz, "A new wireless communication paradigm through software-controlled metasurfaces," *IEEE Commun. Mag.*, vol. 56, no. 9, pp. 162–169, Sep. 2018.
- [14] M. Liu, Q. Yang, A. A. Rifat, V. Raj, A. Komar, J. Han, M. Rahmani, H. T. Hattori, D. Neshev, D. A. Powell *et al.*, "Deeply subwavelength metasurface resonators for terahertz wavefront manipulation," *Adv. Opt. Mater.*, vol. 7, no. 21, p. 1900736, 2019.
- [15] M. Di Renzo, D. Dardari, and N. Decarli, "LoS MIMO-arrays vs. LoS MIMO-surfaces," in *Proc. 17th European Conference on Antennas and Propagation (EuCAP'23)*. Florence, Italy: IEEE, 2023, pp. 1–5.
- [16] M. Akrot, V. Shyanov, F. Bellili, A. Mezghani, and R. W. Heath, "Super-wideband massive MIMO," *IEEE J. Sel. Areas Commun.*, vol. 41, no. 8, pp. 2414–2430, Aug. 2023.
- [17] M. Gao, H. Yin, and L. Han, "An EEP-based robust beamforming approach for superdirective antenna arrays and experimental validations," *arXiv preprint arXiv:2308.11934*, Aug. 2023.
- [18] J. Xie, H. Yin, and L. Han, "A genetic algorithm based superdirective beamforming method under excitation power range constraints," *arXiv preprint arXiv:2307.02063*, Jul. 2023.
- [19] C. Huang, S. Hu, G. C. Alexandropoulos, A. Zappone, C. Yuen, R. Zhang, M. D. Renzo, and M. Debbah, "Holographic MIMO surfaces for 6G wireless networks: Opportunities, challenges, and trends," *IEEE Wireless Commun.*, vol. 27, no. 5, pp. 118–125, Oct. 2020.
- [20] Z. Zhang, L. Dai, X. Chen, C. Liu, F. Yang, R. Schober, and H. V. Poor, "Active RIS vs. passive RIS: Which will prevail in 6G?" *IEEE Trans. Commun.*, vol. 71, no. 3, pp. 1707–1725, Mar. 2023.
- [21] Z. Zhang and L. Dai, "Reconfigurable intelligent surfaces for 6G: Nine fundamental issues and one critical problem," *Tsinghua Sci. Technol.*, vol. 28, no. 5, pp. 929–939, Oct. 2023.
- [22] R. Deng, Y. Zhang, H. Zhang, B. Di, H. Zhang, H. V. Poor, and L. Song, "Reconfigurable holographic surfaces for ultra-massive MIMO in 6G: Practical design, optimization and implementation," *IEEE J. Sel. Areas Commun.*, vol. 41, no. 8, pp. 2367–2379, Aug. 2023.
- [23] K.-K. Wong, A. Shojaeifard, K.-F. Tong, and Y. Zhang, "Fluid antenna systems," *IEEE Trans. Wireless Commun.*, vol. 20, no. 3, pp. 1950–1962, Mar. 2020.
- [24] Z. Zhang, J. Zhu, L. Dai, and R. W. Heath Jr, "Successive Bayesian reconstructor for channel estimation in fluid antenna systems," *arXiv preprint arXiv:2312.06551*, Dec. 2023.
- [25] C. Han, J. M. Jornet, and I. Akyildiz, "Ultra-massive MIMO channel modeling for graphene-enabled terahertz-band communications," in *Proc. IEEE 87th Veh. Technol. Conf. (IEEE VTC'18-Spring)*, Porto, Portugal, Jun. 2018, pp. 1–5.
- [26] O. Yurduseven, D. L. Marks, T. Fromenteze, and D. R. Smith, "Dynamically reconfigurable holographic metasurface aperture for a mills-cross monochromatic microwave camera," *Opt. Express*, vol. 26, no. 5, pp. 5281–5291, 2018.
- [27] Z. Gao, L. Dai, S. Han, C.-L. I, Z. Wang, and L. Hanzo, "Compressive sensing techniques for next-generation wireless communications," *IEEE Wireless Commun.*, vol. 25, no. 3, pp. 144–153, Mar. 2018.
- [28] Z. Wan, Z. Gao, B. Shim, K. Yang, G. Mao, and M.-S. Alouini, "Compressive sensing based channel estimation for millimeter-wave full-dimensional MIMO with lens-array," *IEEE Trans. Veh. Technol.*, vol. 69, no. 2, pp. 2337–2342, Feb. 2020.
- [29] J. Lee, G.-T. Gil, and Y. H. Lee, "Channel estimation via orthogonal matching pursuit for hybrid MIMO systems in millimeter wave communications," *IEEE Trans. Commun.*, vol. 64, no. 6, pp. 2370–2386, Jun. 2016.
- [30] C. Huang, L. Liu, C. Yuen, and S. Sun, "Iterative channel estimation using LSE and sparse message passing for mmWave MIMO systems," *IEEE Trans. Signal Process.*, vol. 67, no. 1, pp. 245–259, Jan. 2019.
- [31] M. Ke, Z. Gao, Y. Wu, X. Gao, and R. Schober, "Compressive sensing-based adaptive active user detection and channel estimation: Massive access meets massive MIMO," *IEEE Trans. Signal Process.*, vol. 68, pp. 764–779, Jan. 2020.
- [32] S. Rangan, P. Schniter, and A. K. Fletcher, "Vector approximate message passing," *IEEE Trans. Inf. Theory*, vol. 65, no. 10, pp. 6664–6684, Oct. 2019.
- [33] N. González-Prelcic, H. Xie, J. Palacios, and T. Shimizu, "Wideband channel tracking and hybrid precoding for mmWave MIMO systems," *IEEE Trans. Wireless Commun.*, vol. 20, no. 4, pp. 2161–2174, Apr. 2021.
- [34] X. Ma and Z. Gao, "Data-driven deep learning to design pilot and channel estimator for massive MIMO," *IEEE Trans. Veh. Technol.*, vol. 69, no. 5, pp. 5677–5682, May 2020.
- [35] X. Ma, Z. Gao, F. Gao, and M. Di Renzo, "Model-driven deep learning based channel estimation and feedback for millimeter-wave massive hybrid MIMO systems," *IEEE J. Sel. Areas Commun.*, vol. 39, no. 8, pp. 2388–2406, Aug. 2021.
- [36] A. Alkhateeb, G. Leus, and R. W. Heath, "Limited feedback hybrid precoding for multi-user millimeter wave systems," *IEEE Trans. Wireless Commun.*, vol. 14, no. 11, pp. 6481–6494, Nov. 2015.
- [37] Z. Xiao, T. He, P. Xia, and X.-G. Xia, "Hierarchical codebook design for beamforming training in millimeter-wave communication," *IEEE Trans. Wireless Commun.*, vol. 15, no. 5, pp. 3380–3392, May 2016.
- [38] T. Zheng, J. Zhu, Q. Yu, Y. Yan, and L. Dai, "Coded beam training," *arXiv preprint arXiv:2401.01673*, Mar. 2024.
- [39] Y. Tsaig and D. L. Donoho, "Extensions of compressed sensing," *Signal Process.*, vol. 86, no. 3, pp. 549–571, Mar. 2006.
- [40] D. L. Donoho, "Compressed sensing," *IEEE Trans. Inf. Theory*, vol. 52, no. 4, pp. 1289–1306, Apr. 2006.
- [41] C. Williams and C. Rasmussen, "Gaussian processes for regression," in *Adv. Neural Inf. Process. Syst.*, vol. 8, 1995.
- [42] N. Srinivas, A. Krause, S. M. Kakade, and M. W. Seeger, "Information-theoretic regret bounds for gaussian process optimization in the bandit setting," *IEEE Trans. Inf. Theory*, vol. 58, no. 5, pp. 3250–3265, May 2012.
- [43] E. Schulz, M. Speekenbrink, and A. Krause, "A tutorial on gaussian process regression: Modelling, exploring, and exploiting functions," *J. Math. Psycho.*, vol. 85, pp. 1–16, 2018.

- [44] G. Zhu, K. Huang, V. K. N. Lau, B. Xia, X. Li, and S. Zhang, "Hybrid beamforming via the Kronecker decomposition for the millimeter-wave massive MIMO systems," *IEEE J. Sel. Areas Commun.*, vol. 35, no. 9, pp. 2097–2114, Sep. 2017.
- [45] D. Tse and P. Viswanath, *Fundamentals of Wireless Communication*. U.K.: Cambridge University Press, 2005.
- [46] T. Cover and J. A. Thomas, *Elements of Information Theory*. New York: Wiley, 1991.
- [47] Y. Sun, P. Babu, and D. P. Palomar, "Majorization-minimization algorithms in signal processing, communications, and machine learning," *IEEE Trans. Signal Process.*, vol. 65, no. 3, pp. 794–816, Feb. 2017.
- [48] J. Song, P. Babu, and D. P. Palomar, "Sequence design to minimize the weighted integrated and peak sidelobe levels," *IEEE Trans. Signal Process.*, vol. 64, no. 8, pp. 2051–2064, Apr. 2016.
- [49] 3GPP TR, "Study on channel model for frequencies from 0.5 to 100 GHz," *3GPP TR 38.901 version 14.0.0 Release*, Dec. 2019.
- [50] C. Meyer, *Matrix Analysis and Applied Linear Algebra*. USA: Society for Industrial and Applied Mathematics, 2000.